Designing Human m_1 Muscarinic Receptor-Targeted Hydrophobic Eigenmode Matched Peptides as Functional Modulators

Karen A. Selz,*†‡ Arnold J. Mandell,*†‡ Michael F. Shlesinger,* Vani Arcuragi,† and Michael J. Owens†
*Cielo Institute, Asheville, North Carolina 28804; †Department of Psychiatry and Behavioral Sciences, Emory University School of Medicine, Atlanta, Georgia 30322; and ‡Department of Mathematical Sciences, Florida Atlantic University, Boca Raton, Florida 33136

ABSTRACT A new proprietary de novo peptide design technique generated ten 15-residue peptides targeting and containing the leading nontransmembrane hydrophobic autocorrelation wavelengths, "modes", of the human m_1 muscarinic cholinergic receptor, m_1AChR. These modes were also shared by the m_4AChR subtype (but not the m_2, m_3, or m_5 subtypes) and the three-finger snake toxins that pseudoirreversibly bind m_1AChR. The linear decomposition of the hydrophobically transformed m_1AChR amino acid sequence yielded ordered eigenvectors of orthogonal hydrophobic variational patterns. The weighted sum of two eigenvectors formed the peptide design template. Amino acids were iteratively assigned to template positions randomly, within hydrophobic groups. One peptide demonstrated significant functional indirect agonist activity, and five produced significant positive allosteric modulation of atropine-reversible, direct-agonist-induced cellular activation in stably m_1AChR-transfected Chinese hamster ovary cells, reflected in integrated extracellular acidification responses. The peptide positive allosteric ligands produced left-shifts and peptide concentration-response augmentation in integrated extracellular acidification response asymptotic sigmoidal functions and concentration-response behavior in Hill number indices of positive cooperativity. Peptide mode specificity was suggested by negative crossover experiments with human m_2ACh and D_2 dopamine receptors. Morlet wavelet transformation of the leading eigenvector-derived, m_1AChR eigenfunctions locates seven hydrophobic transmembrane segments and suggests possible extracellular loop locations for the peptide-receptor mode-matched, modulatory hydrophobic aggregation sites.

A BRIEF DESCRIPTION OF THE CONTEXT FOR THE DEVELOPMENT OF ALGORITHMS FOR RECEPTOR-TARGETED PEPTIDE DESIGN

One-dimensional amino acid sequence pattern analyses

Our laboratory uses one-dimensional, algorithmic signal processing approaches to polypeptide and protein sequence analyses (Mandell, 1984; Mandell et al., 1987, 1997a,b,c, 2000a,b; Selz et al., 1998) and derivative membrane protein-targeted peptide design methods (Mandell et al., 1998a, 2003). These methods have historical roots in Sanger's observation that the uniqueness of polypeptides and proteins lie in their one-dimensional sequence of amino acids (Sanger, 1952), and Anfinsen's conclusion that all the information determining the structure and function of proteins is encoded in the potentially quantifiable physical and chemical properties of their amino acid sequences (Anfinsen, 1973). Our one-dimensional signal processing approach to physical property-transformed amino acid sequences includes the use of wavelet transformations, maximum entropy power spectral transformations, multiple ''ergodic'' entropic measures, and linear decompositions of lagged autocovariance matrices.

Since the introduction of this work, a number of other laboratories have begun to use similar methods of analyses of physical property-transformed amino acid sequences (Giuliani et al., 2003, 2000, 2002; Hirakawa et al., 1999; Lio and Vannucci, 2000; Murray et al., 2002; Rackovsky, 1998). Related matrix methods for sequential pattern finding have been extended to predictions of transmembrane protein structure from nucleotide sequences (Krogh et al., 2001). No others have exploited these techniques for receptor-targeted peptide design. We have recently been granted a United States patent for these and related algorithmic receptor-targeted peptide design methods (Algorithmic Design of Peptides for Binding and/or Modulation of the Functions of Receptors and/or Other Proteins, United States Patent No. 6,560,542, May 6, 2003).

The use of one-dimensional signal processing techniques to reveal patterns in apparently disordered numerical sequences has a long history in fields as diverse as econometrics and meteorology (Bendat, 1958; Box and Jenkins, 1970; Wold, 1965; Yaglom, 1962). More recently this approach has included finding indices of order in apparently disordered, deterministic, chaotic series of quantitative observations (Broomhead et al., 1987; Broomhead and King, 1986; Ott et al., 1994), including biological applications (Guevara et al., 1981; May, 1974), a field with which we have had some experience (Mandell and Russo, 1981; Mandell and Selz, 1997; Russo and Mandell, 1984; Selz and Mandell, 1991; Selz et al., 1995).

This work uses signal processing techniques in the analyses and design of peptide ligands targeting the human m_1 cholinergic, G-protein coupled, seven-transmembrane receptor. These forms of pattern analyses require the transformation of amino acid sequences into numerical series. To do so, we must first choose among quantifiable amino acid physical properties relevant to peptide-protein, noncovalent interactions in aqueous solution. Candidate

Submitted April 4, 2003, and accepted for publication October 23, 2003.
Address reprint requests to Karen A. Selz, E-mail: selz@cieloinstitute.org.
© 2004 by the Biophysical Society
0006-3495/04/03/1308/24 $2.00

physical properties include van der Waals forces, potential for interactions between charged groups, possible relations between the hydrogen bonds of polar groups, and the availability for interactions between nonpolar groups in water, called hydrophobic aggregation (Israelachvilli, 1992).

Choice of a physical quantity for amino acid sequence transformation

Van der Waals interactions occur between aqueous polypeptide groups as well as between these groups and water. The two components are estimated to contribute about equally, and therefore, do not produce a significant net effect in the stabilization of aqueous polypeptide-polypeptide interactions, as in peptide ligand binding or the initial phases of protein folding (Chalaskinski and Szczesniak, 1994; Makhatadze and Privalov, 1993; Privalov, 1987). Amino acid charged groups are statistically relatively rare (Creighton, 1993), and their interactions are shielded by the high dielectric constant, aqueous surround (Bashford and Case, 2000; Ptitsyn et al., 1995; Stillinger, 1977). They are, therefore, assumed to play only a small role in the stabilization of polypeptide interactions (Privalov, 1989; Privalov and Gill, 1988). However, they may play some role in spatially directing the initial phases of protein folding and, analogously, peptide-receptor aggregation (Shoemaker et al., 1997).

Hydrogen bonding occurs between protein polar groups and between these groups and water molecules, leading to only a small net contribution to polypeptide interactional stability (Caflisch and Karplus, 1994; Yang and Honig, 1995). A study of 80 crystallographically characterized protein-ligand complexes, many binding within the nanomolar range, demonstrated no hydrogen bonds between the protein and the ligand. There was, however, a good correlation between lipophioic contact surface in angstroms squared ($Å^2$) and the negative logarithm of their K_i values (Bohm and Klebe, 1996). In addition, using our design algorithms, we have found that the physiologically active, m_1-targeted peptides appear to require a restricted range of average amino acid side-chain pKa values of ≈7.2–7.8 (Table 4, *bottom*). In addition, our recent work indicates that the probability of producing physiologically active autocovariance eigenvector template-generated, de novo peptides can be increased by considering the sequential pattern of receptor sequence's amino acid side-chain pKas (as represented in the relevant pKa autocovariance eigenvector) in the choices of amino acid assignment within its hydrophobic group to the corresponding four-partitioned hydrophobic free-energy eigenvector template (see below for explanatory details).

A commonly held hypothesis is that the greatest source of energy for attractive stabilization of polypeptide-polypeptide or peptide-protein interactions comes from the hydrophobic interactions between the nonpolar groups of amino acid polymers in water (Ben-Naim, 1980; Israelachvili, 1992; Tanford, 1980). This is consistent with more than a half century of work, beginning with Edsall's 1935 observation of an anomalous increase in the molar heat capacity of water in the presence of nonpolar solutes (Edsall and Wyman, 1958), and Franks and Evans (1945) related thermodynamic observations that nonpolar solutes increase the order (decrease the entropy) of water (Franks, 1972). The decrease in entropy that occurs with the transfer of nonpolar groups into water is thermodynamically unfavorable, such that the aqueous system tends to expel these molecules. The expelling action of water on nonpolar groups leads them to aggregate, minimizing their surface area, and this came to be regarded as the general definition of hydrophobic interactions between nonpolar molecules (Kauzmann, 1959; Tanford, 1980). Hydrophobic attraction as measured by atomic force spectroscopy remains significant at distances ≥20 nanometers, and decays more slowly than van der Waals forces with distance (Israelachvilli, 1992; Tsao et al., 1993). These considerations led naturally to our choice of relative amino acid side-chain hydrophobicity as the amino acid parameter for numerical transformation of the targeted G-protein coupled receptor's (GPCR's) sequences, their analyses and the design of GPCR-targeted de novo peptides (Mandell et al., 1998a, 2003).

Choices among and some physical correlates of hydrophobicity scales

There are a large number of experimentally derived numerical scales quantitatively ordering the 20 essential amino acids' relative hydrophobicity in an aqueous environment. Among them are a variety of binary solvent partitions (Cornette et al., 1987; Fauchere and Pliska, 1983; Manavalen and Ponnuswamy, 1978; Nozaki and Tanford, 1971) and relative vapor → water concentrations (Kyte and Doolittle, 1982; Radzicka and Wolfenden, 1988) (see http://pref.etfox.hr./split/scales.html for a relatively complete reference listing with methods used and physical properties quantified leading to 88 hydrophobicity scales). Our computations have demonstrated that interscale correlations ranged from $r = 0.579$ to $r = 0.918$, using a variety of representative solvent partition and vapor pressure determined hydrophobicity scales. Another aqueous solvent-dependent amino acid side-chain property, accessible surface area, in $Å^2$, correlated $r = 0.56$ with the (Eyring-Tanford-Zimmerman) Tanford hydrophobicity scale (Manavalen and Ponnuswamy, 1978) used in these studies. Accessible surface area may be an important physical property with respect to the problem of polypeptide aggregation and binding (Chothia, 1974; Dyson and Wright, 2002a; Huntly et al., 2003). Partial specific volume, in $Å^3$, (Zamyatnin, 1984) and van der Waals volume (volume enclosed by van der Waal radius), in $Å^3$, (Creighton, 1993) correlated with the Tanford hydrophobicity scale as $r = 0.67$ and $r = 0.72$, respectively. The covariation of these properties with the Tanford hydrophobicity scale suggests that the hydrophobic scale, as we have used it, may also

partially address one or more of these hydrophobicity-related properties. Whereas the magnitude of the hydrophobic effect, as measured from the surface area dependence of the solubilities of hydrocarbons in water, has generally been reported to be ~25 calories/mol/Å^2, more recent work taking surface tension at a hydrocarbon-water interface into consideration (Sharp et al., 1991a,b) results in higher estimates of 47 calories/mol/Å^2.

Our research program has used the Tanford scale from the beginning (Mandell, 1984) (Manavalen and Ponnuswamy, 1978) due to its historical precedence, relatively high correlation with most other hydrophobicity scales as well as with other amino acid physical properties, and our previous successes using it in our peptide design algorithms (Mandell et al., 2003). Particularly useful is the Tanford scale's nonarbitrary, four-part partition of the values it gives to the 20 essential amino acids (Manavalen and Ponnuswamy, 1978). These fall into correspondence with the four-partitioned autocovariance eigenvector templates, key elements in our peptide design algorithms.

Proline, which individually partitions with the Tanford scale's most hydrophobic group, behaves like glycine with respect to its influence on secondary structure in x-ray studies of amino acid sequences (Deber et al., 1990; Gunasekaran et al., 1998). Glycine is a member of the Tanford scale's least hydrophobic group. Both are known to disrupt membrane protein secondary structure (Nilsson and von Heijne, 1998; von Heijne, 1991), including turn propensity (Monne et al., 1999) and loops (Duerson et al., 1993; Fetrow et al., 1998). For this reason, we code proline like glycine (0.0 kcal/mol) in the lowest of the natural clusters constituting the four amino acid hydrophobicity groups.

The amino acid sequence of the human m_1 muscarinic cholinergic receptor was obtained from the SWISS-PROT protein sequence data bank. The amino acid hydrophobic free energies in kcal/mol used in these studies divide naturally into four groups (with the above noted proline ''secondary structure breaking'' correction): 1), $G = 0.0$, $P = 0.0$, $Q = 0.0$, $S = 0.07$, $T = 0.07$, $N = 0.09$; 2), $D = 0.66$, $E = 0.67$, $R = 0.85$, $A = 0.87$, $H = 0.87$; 3), $C = 1.52$, $K = 1.65$, $M = 1.67$, $V = 1.87$; and 4), $L = 2.17$, $Y = 2.76$, $F = 2.87$, $I = 3.15$, $W = 3.77$, providing the natural four partitions mentioned above (Manavalen and Ponnuswamy, 1978). These values will be referred to as the Tanford scale.

Sequential patterns, ω^{-1}, in hydrophobicity and secondary structures

Helical turns and β-strands and turns are the best established hydrophobic rotations based on x-ray and NMR evidence of secondary structure, with modes of $\omega^{-1} = 3.6$ amino acids (aa), 2.2 aa, and 2.0 aa, respectively (Eisenberg et al., 1984; Irback et al., 1996; Irback and Sandelin, 2000; Lazovic, 1996; Milner-White and Poet, 1987; Penel et al., 1999; Rose, 1978; Rose and Wetlaufer, 1977; Schiffer and Edmundson, 1967) (see Table 1).

The autocovariance eigenvector modes represent, in effect, a hierarchy of secondary structural, noisy, semiperiodically recurrent, hydrophobic variational wavelengths, ω^{-1}. Our studies of neuropeptides and their receptors have demonstrated dominant hydrophobic wavelengths ranging from $\omega^{-1} = 2.06$ in porins, connexin, and other proteins dominated by up and down antiparallel β-structures (Selz et al., 1998), and $\omega^{-1} = 2.18$ aa in corticotropin releasing hormone, to $\omega^{-1} = 13.6$ aa in acid fibroblastic growth factor in hormonal and neuropeptides (Mandell et al., 1987) to $\omega^{-1} \geq 50$–$70+$ aa in subsequences containing the transmembrane segments of GPCRs (Mandell et al., 1997c). Other examples of dominant hydrophobic wavelengths in protein sequences include: the AIDS viral coat protein manifesting a waxing and waning of hydrophobicity with $\omega^{-1} = 7$–9 aa, a pattern which was conserved across several mutations (Mandell et al., 1987); eigenmodes of representative Ig λ-, κ-, and γ-chains of $\omega^{-1} = 12.5$–13.7 aa (Mandell et al., 1997c); peptide antagonists of the estrogen receptor (Norris et al., 1999) and the ERα estrogen receptor that share a dominant $\omega^{-1} = 8.3$ aa indexed mode (Mandell et al., 2000a); the chaperone GroEL of β-lactamase (Gething, 1997) and β-lactamase, both of which contain leading hydrophobic eigenmode wavelengths of $\omega^{-1} = 16.25$ aa, 4.53 aa, and 2.11 aa (Mandell et al., 2000a). Differences in physical length, as translations of computationally derived hydrophobic variations as wavelengths, are implied by the range of values for the average ''Translation per mode in Å'' seen in the last column in Table 1. These values were computed from amino acid ''Residues per turn'' and ''Translation per residue'' from x-ray crystallographic data (Creighton, 1993).

The role of sequential hydrophobic patterns in peptide-receptor interactions has been demonstrated in studies showing that complete substitution of hydrophobically equivalent amino acids in peptide hormones and neurotransmitters maintains and sometimes increases their peptide-receptor mediated physiological potency (Blanc et al., 1983; Fukushima et al., 1980; Kaiser and Kezdy, 1983; Lau et al., 1983). Self-organizing helical secondary structures of differing average rotational length can be designed with sequences of amino acids that have been binary partitioned

TABLE 1 Hydrophobic modes: rotations and translations

Segment type	Residues per turn (≈mode)	Translation per residue (Å)	Translation per mode (Å)
Antiparallel β	2.0	3.4	6.8
Parallel β	2.0	3.2	6.4
α-Helix	3.6	1.5	5.4
3_{10} helix	3.0	2.0	6.0
π-Helix	4.4	1.15	5.06
Polyproline I	3.3	1.9	6.33
Polyproline II	3.0	3.12	9.36
Polyglycine II	3.0	3.1	9.30

into high and low hydrophobicities, independent of the specific amino acids being chosen within either hydrophobicity class (Kamtekar et al., 1993).

Intermolecular signaling by ω^{-1}-matched hydrophobic sequence attractive aggregation

With respect to the physical chemistry of the eigenmode-matched peptide-protein attraction and aggregation, the hydrophobic attractive force between hydrophobic moieties is a function of surface area and radius of curvature, and can be measured directly using techniques such as atomic force microscopy (Israelachvili and Wennerstrom, 1996). The hydrophobic attractive forces are generally two orders of magnitude greater than those predicted from van der Waals theory, and extend spatially in a slower-than-exponential decay to beyond 20 nm (Pashley et al., 1985). The role of hydrophobic mode matches in attractive aggregation has been observed in the β-strands of interleukin 1β, which bind together and initiate protein folding (Gronenborn and Clore, 1994) in a dynamic process called the ''hydrophobic zipper'' (Dill et al., 1993). Two long helical secondary structures with congruent hydrophobic oscillatory wavelengths bind to form the central ''hydrophobic knot'' that stabilizes the tertiary structure of phospholipase A_2 (Lumry, 1995). The binding of extracellular domains of the growth hormone receptor by polyclonal antibodies to bovine growth hormone is apparently mediated by common sequential hydrophobic variational modes in helical, loop, and disordered secondary structures (Beattie et al., 1996b).

Most of today's approaches to rational peptide ligand design, beyond the high throughput screening of randomly generated peptide libraries (Zysk and Baumbach, 1998), are dominated by pharmacophores, three-dimensional geometric models of proteins' putative active or regulatory binding sites (Guner, 1999; Hruby and Agnes, 1999; Takeuchi et al., 1998). The accelerating increase in the availability of x-ray and NMR characterized three-dimensional structures of proteins might seem to make the use of one-dimensional sequential pattern analyses irrelevant for characterizing peptide-targeted proteins. Polypeptide-protein and protein-protein interactions of physically characterized structures are explored using similar databases and docking algorithms (Janin, 1995; Makino and Kuntz, 1997; Sandak et al., 1998; Stahl and Bohm, 1998). However, an increasing number of studies (Romero et al., 1998, 2001) have demonstrated conformationally disordered polypeptide sequences, particularly relevant to the extracellular loops and juxta-transmembrane subsequences of GPCRs (the targets of our hydrophobic mode targeting peptide design) (Dyson and Wright, 2002a,b; Wright and Dyson, 1999). These subsequences are without stable tertiary structure, as evidenced by missing electron densities in x-ray crystallographic studies, sharp peaks in NMRs, and/or the absence of secondary structural nonlinear Overhauser effects and/or circular dichroism spectroscopic examination with low intensity signals from 210 to 240 nm (Romero et al., 2001). Many of these disordered subsequences become ordered upon ligand binding, going through a disorder-order transition, achieving x-ray and NMR-demonstrable stable tertiary structures (Dyson and Wright, 2002a; Kriwacki et al., 1996; Wright and Dyson, 1999).

Disordered protein subsequences may play significant roles in polypeptide-polypeptide and protein-protein interactions, making them logical targets in rational peptide design (Dunker et al., 1998, 2001; Dunker and Obradovic, 2001). The disordered loop subsequences of globular proteins, 7 transmembrane segment GPCRs, and 12 transmembrane segment membrane transporters (Buck and Amara, 1995; Nirenberg et al., 1997) participate in intramacromolecular signaling as active, allosteric, and antibody binding sites (Bruccoleri et al., 1988; Howl and Wheatley, 1996; Lin et al., 1998; Milner-White and Poet, 1987; Qu et al., 1999; Rondard and Bedouelle, 2000). They may also serve as signal-invoked ''switches'', modulating access to active sites (Branden and Tooze, 1999; Ulloa-Aguirre and Conn, 2000).

MODE SIMILARITIES OF PEPTIDE-TARGETED SUBSEQUENCES OF MUSCARINIC CHOLINERGIC RECEPTOR SUBTYPES AND HYDROPHOBIC MODE-MATCHED MUSCARINIC SNAKE TOXINS

As brief background, there are two classes of acetylcholine receptors. Nicotinic acetylcholine receptors (nAChR) are primarily found in the neuromuscular junctions and autonomic ganglia of the peripheral nervous system, and are cation-selective, ligand-gated ion channel membrane proteins (Unwin, 1993; Wang et al., 2000). In contrast, the muscarinic cholinergic receptors (mAChR) are G-protein coupled, seven transmembrane receptors GPCRs. mAChRs have a 10-fold higher concentration than nAChRs in the brain, and play important roles in attention, arousal, cognition, learning, and memory (Bartus et al., 1982; Flicker et al., 1985; Dickinson-Anson et al., 1998; Fisher et al., 1993; Damasio et al., 1985; Davis et al., 1992).

mAChR's consist of five distinct subtypes, $m_{i,\ i=1,2,\ldots 5}$, categorized by dissimilarities in their amino acid sequences, cholinergic drug-affinities (Bonner, 1989; Bonner et al., 1987; Buckley et al., 1989; McKinney and Coyle, 1991), and differential regional and subcellular distributions in the brain (Adem et al., 1997; Levey, 1996; Mrzljak et al., 1998). Positional alignment of the amino acid sequences of the five mAChR subtypes demonstrates that the greatest differences in segment length occur in the extramembranous amino acids, as well as the terminal carboxy and third intracellular loop, i_3. (Bonner et al., 1987; Liao et al., 1989; Numa et al., 1988; Peralta et al., 1987). The greatest variability in amino acid composition and side-chain sequential physical properties across mAChR subtypes also occurs in the extracellular

loops (e_1, e_2, and e_3) (Hulme, 1990; Hulme et al., 1991). These are the sequence locations of computationally and experimentally demonstrable and differential hydrophobic mode specificities, reflected in the autocovariance eigenvector-generated peptides targeting m_1AChR (and theoretically the mode-equivalent m_4AChR, but not m_2AChR, m_3AChR, or m_5AChR that evidence different dominant hydrophobic modes).

The highly conserved, negatively charged aspartic acid residue in the third transmembrane segment, TM_3 (e.g., D-105 in human m_1AChR and D-111 in human m_4AChR) (Fraser et al., 1989; Hulme et al., 1995) is speculated to bind to the characteristic positively charged headgroups of active site-directed muscarinic ligands (Ehlert and Delen, 1990; Kurtenbach et al., 1990). The hydrophobic, low dielectric constant, membrane interior location of the putative active site on TM_3 is permissive of charge-charge interactions, unlike the high dielectric constant, charge shielded aqueous environments of the e_i and intracellular loops, i_i (Israelachvili and Wennerstrom, 1996; Israelachvilli, 1992; Tsao et al., 1993). We and others have speculated that aqueous environments facilitate the hydrophobic interactions of allosteric and/or indirectly acting peptide ligands with extramembranous portions, e_i, of seven transmembrane receptors (Leckband et al., 1992, 1994; Mandell et al., 2003, 1997c, 2000a; Richards and Richmond, 1977; Tucek and Proska, 1995). Similarly, extracellular hydrophobic interactions with muscarinic GPCRs' e_i are thought to position three-fingered muscarinic snake toxins for their subsequent actions (Jolkkonen et al., 1995; Olianas et al., 1999, 2000).

Noncompetitive modulators of mAChRs exert their positive or negative effects on receptor affinity and/or efficacy via interactions with away-from-the-active-site locations (Birdsall et al., 1995; Jakubik et al., 1996; Lazareno and Birdsall, 1996; Proska and Tucek, 1995). All of the mAChR subtypes are subject to kinetic modulation by a multiple and diverse group of ligands (Birdsall et al., 1997, 1983; Jakubik et al., 1997; Lanzafame et al., 1997; Lee and el-Fakahany, 1991; Proska and Tucek, 1995). Studies using point mutations and chimeral exchanges have indicated that modulatory sites are subject to influence by hydrophobic interactions that involve subsequences in e_i and/or the extramembranous vicinity of the $TM_{i,\ i=1\ldots7}$ (Gnagey et al., 1999; Matsui et al., 1995).

The polypeptide ''fingers'' of the muscarinic three-fingered snake toxins bind in the same locations as the active site-directed ligands, such as atropine and diphenylactoxy-*N*-methylpiperidine (Jolkkonen et al., 1995; Olianas et al., 1999, 2000), but with much higher subtype specificity (Kukhtina et al., 2000). The small differences in the dissociation constants in $-\log(K_d)$ for atropine studied in murine muscarinic receptor transfected fibroblasts have been reported as: $m_1 = 9.29$, $m_2 = 9.00$, $m_3 = 9.28$, $m_4 = 9.66$, and $m_5 = 9.43$, and for diphenylactoxy-*N*-methylpiperidine, 4-DAMP, $m_1 = 8.92$, $m_2 = 8.21$, $m_3 = 9.19$, $m_4 = 9.15$, and $m_5 = 8.92$ (Kashihara et al., 1992). The failure of these active site-targeted small molecule cholinergic agents to discriminate among muscarinic receptor subtypes contrasts with the high selectivity of the m_1 and m_4 muscarinic receptor polypeptide ''three-finger'' snake toxins. The values of their inhibition constants, $K_i = IC_{50}/(1+[L]/K_d)$ in nM of [^{3}H]-*N*-methyl-scopoline binding in human mAChR-transfected Chinese hamster ovary (CHO) cells are: $m_1 = 0.2$–48.0 and $m_4 = 2$–120 vs. m_2, m_3, and $m_5 = >1000$–$20{,}000$, the members of this snake toxin family being the most m_1 and m_4 receptor selective ligands known. (Adem and Karlsson, 1997).

The amino acid sequence analyses and GPCR-targeted, modulatory peptide designs presented here focus on the sequential hydrophobic patterns that are statistically dominant after the hydrophobic variation due to the transmembrane segments is computationally removed. m_1AChR and m_4AChR were found to share ''hydrophobic modes'' that differed from those evidenced in the m_2, m_3, and m_5 subtypes (see Table 3). The modes shared by the m_1 and m_4 muscarinic cholinergic receptors were also dominant in the family of three-fingered muscarinic snake toxins which bind with specificity to those receptor subtypes (see Table 2).

SEQUENTIAL MODE ANALYSES IN THE HYDROPHOBICALLY TRANSFORMED AMINO ACID SEQUENCE OF M_1ACHR: BACKGROUND, METHODS AND FINDINGS

Patterns of hydrophobic variation in secondary structure

It has long been known that sequential patterns in amino acid hydrophobic variation, recurrent patterns we call hydrophobic modes, can contribute to the prediction of secondary and supersecondary structures and their interactions in globular and membrane proteins (Chothia, 1975; Chothia and Janin, 1975; Chou and Fasman, 1974a,b; Cornette et al., 1987; Rose, 1978; Rose and Roy, 1980; Rose and Wetlaufer, 1977; Schiffer and Edmundson, 1967). These patterns have been characterized using a variety of descriptions of sequential hydrophobic variation, sometimes including smoothing by nearest neighbor averaging of amino acid hydrophobicities (Kyte and Doolittle, 1982). Among the best known of the hydrophobic mode descriptors are Edmondson's amphipathic helical wheel (Kaiser and Kezdy, 1983; Schiffer and Edmundson, 1967), Eisenberg's hydrophobic moments (Eisenberg et al., 1984), Rose's chain turns (Rose, 1978), Skolnick's β-turns (Godzik and Skolnick, 1992), and Fourier and wavelet transformations in hydrophobic wavelengths (Eisenberg et al., 1984; Giuliani et al., 2000, 2002; Hirakawa et al., 1999; Lazovic, 1996; Lio and Vannucci, 2000; Mandell, 1984; Mandell et al., 1987, 1997a,b,c; Murray et al., 2002; Rackovsky, 1998; Selz et al., 1998).

Our findings suggest hydrophobic mode-selective attractive aggregation between polypeptide ligands and e_i, juxta-TM_i receptor, and other subsequences containing matching modes (e.g., chaperone-protein binding) (Mandell, 1984; Mandell et al., 1998a, 1987, 1997c, 2000a,b). As noted above, these phenomena appear analogous to the self-aggregation of sequential, amphipathically matching amino acid sequences in a process called ''hydrophobic zippering'' (Dill et al., 1995, 1993; Gronenborn and Clore, 1994), a process hypothesized to initiate folding in many proteins. Similarly, helical bundle formation is known to occur along the long axes of amphipathic helices with matching hydrophobic modes (Gibney et al., 2000; Park et al., 2000; Shu et al., 2000).

TABLE 2 Dominant hydrophobic wavelengths of snake muscarinic toxins

MT-1	MT-2	MT-3	MT-4	MT-5	MT-7	MT-α	MT-β
2.59, 7.69	2.79, 8.36	7.70, 2.76	2.59, 7.83	2.73,7.72	2.51, 7.59	2.60, 7.63	2.61, 7.81

Characteristic wavelengths of hydrophobic recurrence (modes) in polypeptides

Generalizing the above suggestive relationships between patterns of hydrophobic variation and x-ray determined secondary structures in proteins, and exploiting the evolutionary statistical stationarity of polypeptide and protein sequence structure that justify the use of signal processing techniques on short series lengths, our laboratory used methods including Fourier and moving window Fourier transformations to elucidate familial mode commonalities in hormonal and neural peptides (Mandell, 1983, 1984, 1986, 1987; Mandell et al., 1987). For instance, a family of trophic peptide hormones with <50% sequence homology, growth hormone releasing factor, glucagon, vasoactive intestinal peptide, PHI, somatoliberin, and the A-chain of insulin, were found to share a dominant hydrophobic mode of $\omega^{-1} = 4.0$ aa wavelength (Mandell et al., 1987). Attempts to find mode matches by applying these techniques to the >400-aa-long sequences of their and other membrane receptors were only occasionally successful; for example, there appeared to be mode matches between several nicotinic cholinergic toxins and nicotinic cholinergic receptors in the electric organ of the Torpedo ray. Generally, however, even the 50-residue windowed moving Fourier power spectra of the hydrophobic transformed sequences of receptor sequences were ambiguous. The spectra were dominated by the high amplitude, long wavelength, $\omega^{-1} \approx 50$–$70+$ aa variation of the highly hydrophobic transmembrane segments. The spectra were noisy, with difficult-to-localize broadband peaks, manifesting end effects and often multiperiodic. All of these problems made an examination for peptide ligand and receptor hydrophobic mode matches difficult.

Orthogonal mode decomposition augments power spectral techniques in elucidating hydrophobic modes in GPCRs

The evolutionary stationarity of what would otherwise be considered too-short GPCRs aa series length for statistical treatment, the Wiener-Khinchine relations (Bendat and Piersol, 1986) associating the correlation and spectral density functions (with spectra already found promising for characterizing hydrophobic modes in shorter hormonal and neuropeptide series), and the need to deal with the sources of poor mode definition listed above, led naturally to the selection of techniques derived from principle component analyses (Fukunaga, 1990). These methods involve the linear decomposition of correlation matrices and allow the computational removal of the dominant transmembrane hydrophobic pattern, the discrimination of the remaining leading modes from the noise floor, and the isolation of the leading orthogonal modes from each other in potentially multimodal patterns. Being without end effects and other potential limitations of fixed transforms (e.g., of Fourier or Bessel), these transformations individually tailor the ''shape'' of the mode representation to the specific data series (in the form of the leading eigenvectors, X_i, of the series' lagged autocovariance matrices) (Brillinger, 1981; Broomhead et al., 1987; Broomhead and King, 1986). In the following, please notice that the computationally derived hydrophobic mode(s) of GPCRs are represented in most detail by the leading eigenvectors, X_i, singular or summed, of the lagged autocovariance matrix transformation of the original hydrophobic series (Broomhead et al., 1987; Broomhead and King, 1986; Golub and Van Loan, 1993) (see below). They are represented more generally by an approximating index, ω^{-1} in aa, by the maximum entropy, all-poles power spectral transformations (which picks out one or two leading ω-values) (Press et al., 1988) of the leading X_i or of a constructed new smoothed function formed by the serial composition of X_i with the original amino acid hydrophobic series to form an eigenvector-weighted nearest neighbor-averaged autocovariance matrix eigenfunction, ψ_i (Broomhead et al., 1987; Broomhead and King, 1986).

TABLE 3 Hierarchy of hydrophobic wavelengths in m_iAChR

	Receptor				
$\Psi_{i,\ I\ =\ 1\ldots15}$	m_1	m_2	m_3	m_4	m_5
1	~73	~90	~90	~74	~66
2	7.78	2.00	3.14	40	8.66
3	7.74	8.70	11.05	7.04	2.00
4	2.42	8.57	11.62	7.84	7.94
5	2.43	5.06	3.12	2.37	3.96
6	12.05	13.89	2.56	4.69, 2.44	3.87
7	5.73	14.01	2.60	4.71	14.08

Methods of lagged autocovariance matrix formation, eigenvector extraction, and autocovariance matrix eigenfunction construction from m_1's hydrophobic series

The hydrophobically transformed amino acid sequences were used to generate an M-lagged data matrix from which $M \times M$ covariance matrices, C_M, were computed. These C_M were decomposed into sets of l orthogonal eigenfunctions, $\psi_{l(j),\ l\ =\ 1\ldots M,\ j\ =\ 1\ldots n\ -\ M+1}$ (Broomhead et al., 1987; Broomhead and King, 1986; Golub and Van Loan, 1993).

More specifically, from the sequentially lagged data column vectors ($T \equiv$ transpose) $V_1{}^T = (H_1, H_2 \ldots, H_{n-M})$, $V_2{}^T = (H_2, H_3, \ldots, H_{n-M+1})$, …, $V_M{}^T = (H_M, H_{M+1,\ldots,} H_n)$ and where $K = n - M + 1$, the sequence-averaged dyadic product, $H_i H_i{}^T$ is used to obtain the autocovariance matrix, a Hermitean $M \times M$ matrix, $C_M = 1/K\{H_i H_i{}^T\}$. $M = 15$ was chosen for the m_1 muscarinic cholinergic receptor to minimize the least-squares error of m_1's leading ψ_1, representing the pattern of the highly hydrophobic transmembrane segments, and the m_1 receptor's nearest neighbor-smoothed hydropathy plot, which is also dominated by the transmembrane pattern (Kyte and Doolittle, 1982). We compute the ordered eigenvalues, $\{\nu_i\}_{i\ =\ 1\ldots M}$, and the associated ordered eigenvectors, $X_i(j)$, of C_M, where $i = 1\ldots M$ and labels the eigenvector, and $j = 1\ldots M$ and refers to the jth components of the eigenvector X_i. The $\{\nu_i\}_{i\ =\ 1\ldots M}$ are ordered from largest to smallest and constitute the eigenvalue spectrum of C_M. The similarly ordered associated $X_i(j)$ are convolved with original hydrophobic series into their associated eigenfunctions $\psi_l(j)$, where $l = 1\ldots M$ labels the eigenvector and $j = 1\ldots n - M$ indexes the eigenfunction's jth component. That is, the convolution of each of the leading eigenvectors with the hydropathy series is carried out by computing the sums of the scalar products of the M length eigenvector with an M length of the hydrophobic series to produce a point in the eigenfunction; this process is translated down the data series by one step and repeated to generate each of the sequential points of the eigenfunction that corresponds to its ordered eigenvalue-associated eigenvector in the computation. In those studies, the ψ_l of M are plotted as a function of the M lag-reduced sequence position.

Intuitively, C_M scans for hydrophobic modes across a range of autocorrelation lengths from 1 to M, the range of the lags defined in the original data matrices and reflected in the autocovariance matrices. Because C_M is real, symmetric and normal ($C_M C_M{}^T = C_M{}^T C_M$), its $\{\nu_i\}_{i=1\ldots M}$ are real, nonnegative, and distinct, and its associated $X_i(j)$ constitute a natural basis for orthonormal projections on m_1's hydrophobic series (Golub and Van Loan, 1993). The set of ψ_l can be regarded as orthonormally decomposed sequences of eigenvector-weighted, moving average values (Broomhead et al., 1987; Broomhead and King, 1986).

All-poles maximum entropy power spectral transformation of the leading eigenfunctions

The ψ_l were transformed into their dominant hydrophobic modes (inverse frequencies, ω^{-1}) using all-poles maximum entropy power spectra, $S_\omega(\psi_l)$ (Madan, 1993; Press et al., 1988)). Generally, $S(\omega) = a_0/|1+\Sigma_{k=1\ldots M} a_k \exp(ik\omega)|^2$, such that the zeros of the denominator result in peaks (''poles'') marking the dominant hydrophobic mode(s) of the ψ_l. This form of the Fourier transformation generates relatively well-resolved spectral peaks in finite series in which only a small number, k, of the (auto)covariance coefficients, c_k, are known. In these studies, $k \leq 8$ to avoid ''splitting'' $S(\omega)$ into spurious modes. The Fourier coefficients, a_k , can be calculated from the set of data-derived c_k, chosen so that the entropy of the spectral estimate, $h = \int \ln S(\omega^{-1}) d\omega$, is maximal. Beyond the limited information of the small set of data-derived autocorrelation-matched Fourier coefficients, called the ''correlation matching property'', the process is extended into a Gaussian process such that h is maximized. It is known that the Gaussian is the function that maximizes h under the constraints of a finite number of second order c_k, as in our data (Madan, 1993). Intuitively, the all-poles maximum entropy $S(\omega)$ yields results like an autoregressive, maximum likelihood spectral estimate in that it is not model-dependent, but rather its a_k values follow from the c_k values that are derived directly from the data (Priestly, 1981). This technique acts as a filtering process, yielding the moduli of the one or two leading complex poles of discrete hydrophobic variational frequency in minimally distorted form from the leading ψ_l of the lagged autocovariance matrix of the m_1 sequence (Mandell et al., 1998a, 1997a,b,c; Selz et al., 1998).

The transmembrane mode as an example: the leading eigenfunction, ψ_1, of the m_1 lagged autocovariance matrix, C_M, and its all-poles power spectral representation, $S_\omega(\psi_1)$

To exemplify the results of computational hydrophobic mode extraction, we compare the standard m_1 smoothed hydropathy plot with the X_1 determined (convolved with the original sequence) leading eigenfunction, ψ_1, and its all-poles power spectral transformation, representing the transmembrane mode of the m_1 muscarinic cholinergic receptor (Giuliani et al., 2002; Mandell et al., 1998a, 1997c). Fig. 1 *A* is a plot of the hydrophobically transformed amino acid series of m_1 using the Tanford scale as listed above (Manavalen and Ponnuswamy, 1978). Fig. 1 *B* is the all-poles power spectral transformation of the hydropathy plot of Fig. 1 *A* evidencing its noisy floor, broadband peaks, and multimodality, all of which make the isolation and characterization of its hydrophobic modes not possible. Fig. 1 *C* was computed by a nearest-neighbor, three-point moving average of the hydrophobically transformed m_1 amino acid sequence, iterated 11 times and plotted as a function of the m_1-11 length adapted from the approach of Kyte and Doolittle (1982). Five-point moving averages iterated 11 times were used to test the stability of the pattern of its hydrophobic oscillations. Fig. 1 *D* is a graph of the all-poles power spectral transformation of Fig. 1 *C* demonstrating its long wavelength of $\omega^{-1} = 71.43$ aa. Fig. 1 *E* is a graph of m_1's ψ_1 that very closely resembles the pattern of hydrophobic oscillations of the transmembrane mode in the graph of Fig. 1 *C*. Fig. 1 *F* is a graph of the all-poles maximum entropy power spectral transformation of m_1's ψ_1, indicating its long hydrophobic wavelength, $\omega^{-1} = 73.15$ aa. Note that the spectrum of the leading eigenfunction differs by <2% in the frequency-wavelength domain from that of the nearest neighbor-averaged hydropathy plot (Fig. 1 *D*).

We graph the results of this computation of m_1's transmembrane mode to exemplify the above outlined methods used in hydrophobic mode extraction and characterization using the all-poles power spectra of the C_M's X_i-defined hierarchy of leading hydrophobic modes (Mandell et al., 2001, 1997c; Selz et al., 1998). As described above, the maximum lag described in the autocovariance matrix, here 15, determines the length of the eigenvalue-weighted eigenvector(s) used as templates for amino acid assignment in peptide design (see below). This value is chosen from a range of values so as to maximize the correlation between the leading eigenfunction, ψ_1 (Fig. 1 *E*), and the nearest neighbor-averaged hydropathy plot (Kyte and Doolittle, 1982) (Fig. 1 *C*) (Mandell et al., 1997c).

Hydrophobic mode hierarchies in the family of muscarinic cholinergic receptors, m_iAChR: characteristic m_1 and m_4 modes

Using the methods illustrated above for the isolation and characterization of the m_1 transmembrane mode, Table 3 lists the all-poles power spectral hydrophobic mode wavelengths ω^{-1} of the ordered leading eigenfunctions, ψ_i, of the five human m_iAChR subtypes. The m_1 and m_4 subtypes share hydrophobic eigenfunction modes of $\omega^{-1} \approx 7.8$ aa and 2.4 aa, neither of which are present in the other three mAChR subtypes. Note that the closest to these values of these three is the 7.94 aa mode of the m_5 subtype. This m_5 mode demonstrates a difference from the m_1 target of >2% in the frequency-wavelength domain (compare with <2% mode similarity comparing the nearest neighbor-averaged and eigenfunction representations of the transmembrane mode). Two percent or less difference is our approximate criteria for declaring mode frequency-wavelength similarities and differences. Power spectral modes of the eigenfunctions associated with the 8th through the 15th ordered eigenvectors are not shown. The receptors' eigenvalue spectra decayed quickly, and values of λ_7 through λ_{15} were very small, accounting for very little of the receptors' variance in hydrophobic free energy.

When a cell in Table 3 contains two entries—for example, the power spectral peaks of ψ_6 in m_4—it is because a single eigenfunction, here ψ_6, evidenced the indicated two well-defined peaks that were of nearly equivalent power. The other kind of redundancy sometimes demonstrated within a single receptor subtype results from isomodal eigenfunctions that are out of phase and therefore orthogonal. In those cases, we see two eigenfunctions with approximately the same statistical wavelength and usually with similar eigenvalues and relative spectral power. An example of this is also seen in Table 3, where the second and third eigenfunctions of m_1AChR (ψ_2 and ψ_3) manifest an isomodal, out-of-phase redundancy. Generally in such cases, the eigenfunction associated with the slightly larger eigenvalue is chosen in the construction of the receptor-targeted peptide template.

As in our previous work (Mandell et al., 2003, 1997a,b,c, 1998b; Selz et al., 1998), the dominant wavelengths of the power spectral modes of m_1AChR's ψ_i values were confirmed and localized in the receptor sequence with reference to the dominant mother wavelet scales and their sequence locations using continuous, one-dimensional Morlet wavelet transformations (Farge et al., 1993; Strang, 1993; Wickerhauser, 1994). These demonstrated that the sequence locations of the mother wavelet scale density centroids corresponding to the ≈7.8 aa power spectral mode of ψ_2 (and isomodal but phase-advanced ψ_3) were in the sequence vicinity of the putative e_1 and e_3 extracellular loops. (See Fig. 3 *B* and associated discussion below.) This finding is relevant to the modulatory role of hydrophobic mode matches in these sequence locations because alanine mutagenesis of Tyr-101 and Tyr-404, in the e_1 and e_3 loops, respectively, resulted in the m_1 allosteric ligands, gallamine and himbacine, failing to bind and/or modulate the m_1

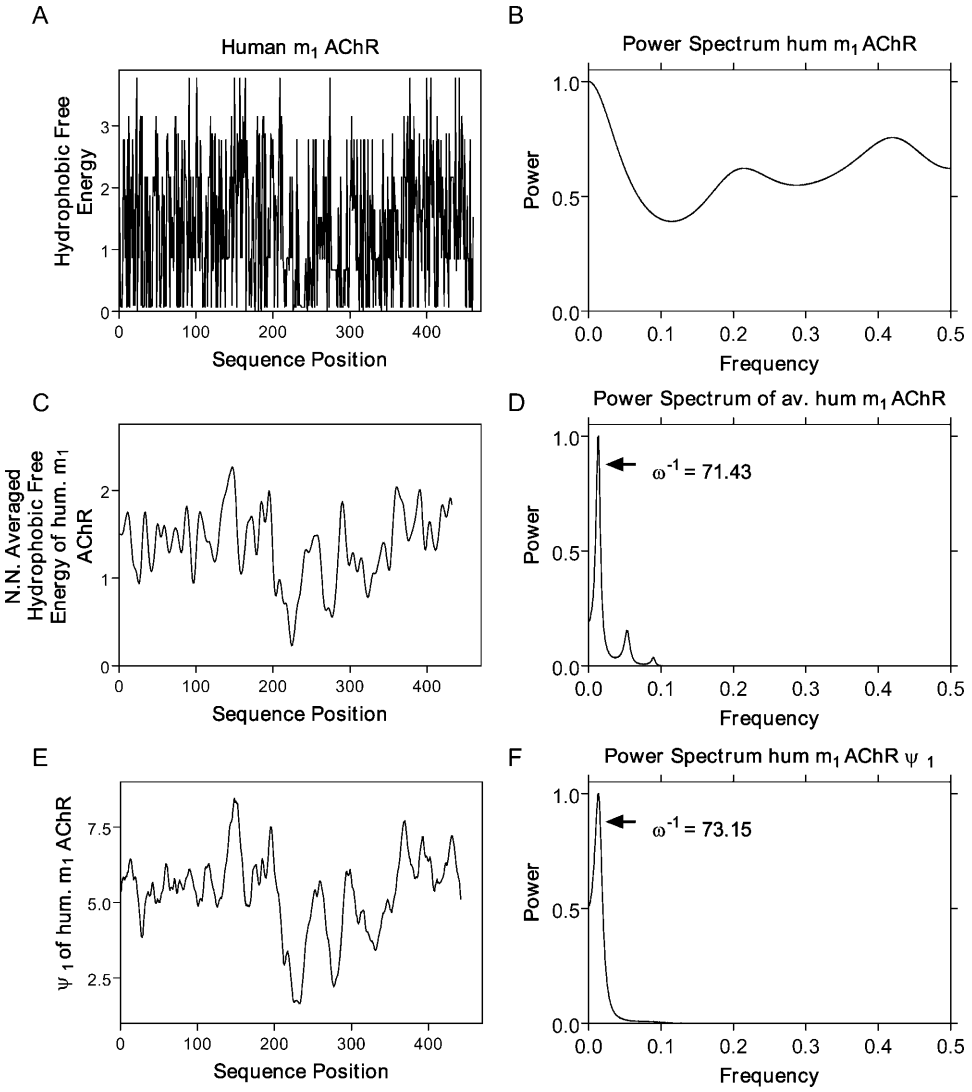

FIGURE 1 (*A*) Plot of the hydrophobically transformed amino acid series of m_1AChR using the Tanford scale (kcal/mol). (*B*) All-poles power spectral transformation of the series in *A*. *A* is an undecomposed sequence and results in a noisy, multimodal spectrum with broadband peaks, complicating the isolation and characterization of its hydrophobic modes. (*C*) Results of an iterative nearest-neighbor, three-point moving average transformation of the hydrophobically transformed series in *A*. (*D*) All-poles power spectral transformation of the series shown in *C*, demonstrating its dominant long hydrophobic wavelength of $\omega^{-1} = 71.43$ aa. m_1AChR's hydrophobically transformed series is used to produce a sequentially lagged data matrix. The autocovariance matrix of this data matrix is computed and its eigenvalues and eigenvectors are derived. (*E*) m_1AChR's leading eigenfunction, ψ_1, resulting from a linear decomposition of its lagged autocovariance matrix, after which the eigenvector associated with the largest eigenvalue of the autocovariance matrix is composed with the original hydrophobic series shown in *A*. Note that m_1AChR's ψ_1 very closely resembles the pattern of hydrophobic oscillations seen in the nearest-neighbor hydropathy plot that is known to be dominated by the pattern of hydrophobic transmembrane segments (*C*). (*F*) All-poles, maximum entropy power spectral transformation of ψ_1, indicating its long dominant hydrophobic wavelength, $\omega^{-1} = 73.15$ aa, which differs by $<2\%$ in the frequency-wavelength domain from that of the nearest neighbor-averaged hydropathy plot (*D*). Maximum lag in the data matrix determines the dimensions of the autocovariance matrix and the length of the eigenvectors and of the peptides built from the eigenvector template (see text). Here we chose that value to be 15, the value <25 that minimized least-squares error in the fit of ψ_1 with the nearest neighbor-averaged hydropathy plot (*C*) to ψ_1 (*E*).

muscarinic receptor (Matsui et al., 1995). The e_i are known to be common locations for ligand-mimetic binding of antibodies raised to transmembrane receptors (Beattie et al., 1996a,b). Molecular dynamics simulations of protein motions show coupling between peptide chain loops (Watanabe et al., 1997), and such modulation of loop movements can serve as ''molecular switches'' (Ma and Karplus, 1997) initiating conformational transitions in some proteins (Lazaridis and Karplus, 1997).

Hydrophobic modes in a family of muscarinic snake toxins: similarities with the characteristic m_1 and m_4 leading hydrophobic modes

As an independent source of mAChR-matched hydrophobic modes, we studied the family of 64–65 residue peptide toxins from the green and black mamba snakes, *Dendroaspis angusticeps* and *Dendroaspis polylepis* (Jerusalinsky et al., 1997; Jerusalinsky and Harvey, 1994). These toxins have been shown to be selectively specific for the m_1 and m_4, but not m_2, m_3, or m_5 AChR subtypes. They manifest long-lasting ''pseudoirreversible'' allosteric modulation of muscarinic antagonist binding (Adem et al., 1997; Adem and Karlsson, 1997). The leading hydrophobic modes of the all-poles power spectral transformation of these relatively short, 64–65 residue hydrophobically transformed amino acid series are listed in Table 2. Because of their short lengths and the absence of TM associated modes, the toxins did not require eigendecomposition of their autocovariance matrices. MT-1 through MT-7 are m_1AChR and m_4AChR subtype specific muscarinic toxins isolated and sequenced from the venom of the green mamba (Adem and Karlsson, 1997; Olianas et al., 2000). MT-α and MT-β were isolated and sequenced from the venom of the black mamba snake (Adem and Karlsson, 1997; Jerusalinsky et al., 1997; Olianas et al., 2000). Note how the two dominant hydrophobic modes of the m_1 and m_4 specific snake toxins approximate the dominant modes found in the posttransmembrane hydrophobic modes of the m_1 and m_4 receptors (Table 3). We note that these hydrophobic modes are not generic for all three-fingered toxins in that all of the members of the three-fingered nicotinic acetylcholine receptor-targeted toxins of sea kraits demonstrate dominant hydrophobic wavelengths of 2.0 and $\approx$4.15 aa (Housset and Fontecilla-Camps, 1996).

DESIGN OF M_1ACHR-TARGETED PEPTIDES USING LEADING EIGENVECTOR MODES AS TEMPLATES FOR POSITIONAL ASSIGNMENT OF AMINO ACIDS BY HYDROPHOBIC GROUP

This algorithmic approach to m_1AChR-targeted peptide design contrasts with many other rational peptide design strategies that exploit geometric, active site models of physiologically active peptides called ''pharmacophores'' (Hruby and Agnes, 1999; Takeuchi et al., 1998; Zysk and Baumbach, 1998). These models are composed of three-dimensional arrangements of molecular constituents with potential noncovalent interactions, including hydrogen bond donors and acceptors, ionizable groups, and ring or chain hydrophobic aggregation. Models emphasize modular components found to be common among similarly active agents. These are often discovered by high through-put screening of large peptide libraries (Guner, 1999).

In contrast, our sequence approach to the hydrophobic mode characterization of GPCRs is uniquely relevant to membrane protein subsequences that may be without stable tertiary structure (Romero et al., 1998). As described above, these conformationally disordered polypeptide sequences evidenced in x-ray crystallographic studies by missing electron densities, nuclear magnetic resonance graphs with sharp peaks, and/or the absence of evidence for secondary structure in nuclear Overhauser effects and circular dichroism studies with low-intensity signals from 210 to 240 nm (Dyson and Wright, 2002a,b; Romero et al., 2001; Wright and Dyson, 1999). Such subsequences characteristically become ordered upon ligand binding, going through a disorder-order transition and achieving x-ray and/or NMR demonstrable stable tertiary structure (Dyson and Wright, 2002a,b; Kriwacki et al., 1996; Wright and Dyson, 1999).

Recall that disordered loop sequences of globular proteins, GPCRs, and 12 transmembrane segment transporters (Buck and Amara, 1995; Nirenberg et al., 1997) have been shown to play significant roles in polypeptide-polypeptide and protein-protein interactions, participating in allosteric and antibody binding sites (Rondard and Bedouelle, 2000) and modulatory ''switches'' (Ulloa-Aguirre and Conn, 2000). This makes them promising targets in rational peptide ligand design (Dunker et al., 1998, 2001; Dunker and Obradovic, 2001). We address these targets, using the leading hydrophobic eigenvector(s), X_i, in mode-matched polypeptide ligand design. In this way, we have successfully targeted ''away from the active site'' GPCR modulatory mechanisms in the D_2 dopamine receptor (Mandell et al., 2003; Naylor et al., 1995; Simpson et al., 1999; Vaughan et al., 2001) and the nerve growth factor tyrosine kinase receptor (Mandell et al., 2001). After computational removal of the transmembrane mode (Fig. 1), the leading eigenvector hydrophobic modes tend to be concentrated in putative extracellular loop and juxta-transmembrane polypeptide subsequences in membrane receptors (Mandell et al., 1998a, 2003, 2001, 1997c). As noted above, our initial studies using this approach to analyses found many autocovariance matrix eigenvector-determined hydrophobic mode matches between naturally occurring hormonal and neuropeptides and their receptors (Mandell et al., 1998a,c). Based on hydrophobic mode matches we have predicted polypeptide-protein interactions later found in a chaperone and its associated protein, as well as in peptide modulators of the estrogen receptor and the receptor itself (Mandell et al., 2000a).

The design process involves the use of the posttransmembrane, leading, lagged autocovariance matrix, eigenvalue-weighted eigenvector(s). These eigenvectors are four-equipartitioned to correspond to the natural four clusters of hydrophobicity in the Tanford scale, and used as templates for amino acid assignment. Amino acid assignment is made by group/partition as weighted by their probability of occurrence (in each hydrophobic group) as measured in the human brain's extracellular fluid (Perry et al., 1975). In the study designing physiologically active peptides targeting the tyrosine kinase-coupled, nerve growth factor tyrosine kinase receptor (without the seven transmembrane mode of GPCRs), the receptor manifested three orthogonal leading eigenvector modes, X_1, X_2, and X_3, which, being almost equal in modular amplitude and linearly independent, were combined in an eigenvalue-weighted sum to generate the template for amino acid assignment (Mandell et al., 2001). In designing the physiologically active D_2DAR-targeted peptides (Mandell et al., 2003), the transmembrane mode was computationally removed. The two leading posttransmembrane hydrophobic modes were both found in ψ_2, and the associated X_2 was used as the template for probability-weighted amino assignment. After computational removal of the transmembrane mode of m_1AChR (Fig. 1, *E* and *F*), there were two leading eigenvector modes remaining: one found in ψ_2, $\omega^{-1} = 7.78$ aa (Fig. 2, *A* and *B*; Table 3) and its phase shifted near redundancy in ψ_3, $\omega^{-1} = 7.74$ aa (Table 3). The other was found in ψ_4, $\omega^{-1} = 2.42$ aa (Fig. 2, *C* and *D*) and its phase shifted near redundancy in ψ_5, $\omega^{-1} = 2.43$ aa (Table 3).

Based on these findings, the eigenvector template was constructed from the sum of the second eigenvalue weighted X_2 (associated with ψ_2) and the fourth eigenvalue weighted X_4 (associated with ψ_4). This four-partitioned eigenvector m_1 template (Fig. 2 *E*) was used in the design of the m_1AChR-targeted, 15 mer peptides as listed in Table 4. The template sequence by partition section is listed, with lowest to highest hydrophobicity group represented numerically as 1, 2, 3, and 4. As noted above, in each of the 15 template locations, an amino acid representative of its matching hydrophobic group was randomly assigned, as probabilistically weighted by its (within group) occurrence in human brain extracellular fluid (Perry et al., 1975) (Fig. 2 *E*). Of the peptides computationally generated by the iterative application of this procedure, we selected the 10 amino acid sequences for synthesis to

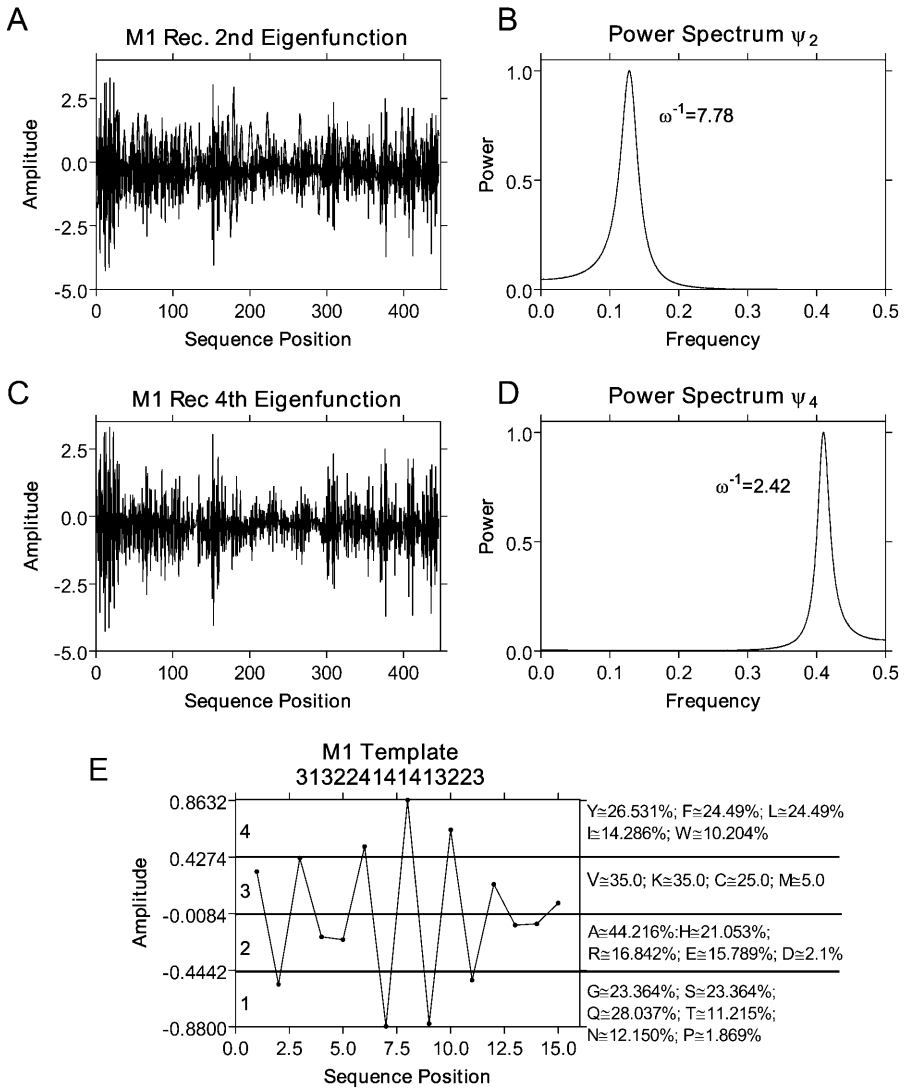

FIGURE 2 (*A* and *C*) m_1AChR's second and fourth hydrophobic free energy eigenfunctions, ψ_2 and ψ_4, constructed by the composition of the second and fourth largest eigenvalued eigenvectors, X_2 and X_4, of its 15-lagged autocovariance matrix, with the hydrophobic series of the human m_1 muscarinic receptor (shown in Fig. 1 *A*). m_1AChR's third and fifth eigenfunctions, ψ_3 and ψ_5, were phase-shifted versions of ψ_2 and ψ_4, respectively (see Table 3). The leading eigenfunction, ψ_1, was dominated by the pattern of seven transmembrane segments (shown in Fig. 1, *E* and *F*). (*B* and *D*) All-poles power spectral transformations of ψ_2 and ψ_4. Their dominant hydrophobic variational frequency peaks correspond to hydrophobic mode wavelengths of $\omega_2^{-1} = 2.42$ aa and $\omega_4^{-1} = 7.78$ aa. (*E*) Eigenvector template constructed as the eigenvalue weighted sum, $\lambda_2 X_2 + \lambda_4 X_4$, where λ_i are the autocovariance matrix-ordered eigenvalues. The template was four-equipartitioned to correspond to the amino acids' four hydrophobic groups. In the peptide design process, specific amino acids are assigned randomly within these groups, as distributionally weighted by within-group membership in the human brain's aqueous amino acid pool. *E* also indicates amino acid groups' membership and their approximate within-group probabilities of occurrence in human cerebrospinal fluid.

≥95% purity (by mass spectrometry) by Multiple Peptide Systems (La Jolla, CA) (Table 4) that manifested all-poles power spectral wavelengths that deviated least from the dominant wavelengths of ψ_2 and ψ_4 (Fig. 2, *B* and *D*) and the muscarinic snake toxins (Table 2).

LOCATING PUTATIVE ALLOSTERIC SITES BY REPRESENTING THE M_1ACHR'S LEADING EIGENVECTOR MODES AS MODULAR DENSITIES IN THE MORLET WAVELET PLANE

Rhodopson, whose x-ray structure is now known at 2.8 Å resolution (Palczewski et al., 2000) is perhaps generalizable to other GPCRs, but very little specific has been established about the locations and characteristics of other GPCR's orthosteric or allosteric sites (Schwartz and Rosenkilde, 1996). Studies using point mutagenesis, chimeric exchanges, and chemical modifications of putative sites have shown a diversity of apparent orthosteric and allosteric binding domains, including those within the transmembrane regions (for many biogenic amines), those involving both transmembrane, TM_i, and extracellular loop, e_i, subsequences (for some neuropeptides) and those in the N-terminal domain (for some neuropeptides and metabotropic ligands) (Christopoulos and Kenakin, 2002).

Unlike Fourier transformation, wavelet transformations of hydrophobically coded protein receptor amino acid series conserve information about both sequence location and hydrophobic eigenmode wavelength (Daubechies, 1992; Farge et al., 1993; Mallat, 1989; Wickerhauser, 1994). Using discrete, best basis, trigonometric wavelet transformations, we have confirmed the power spectral leading eigenvector mode matches of several opiate peptides with their receptors and of somatostatin, bombesin, neurotensin, and cholecystokinin with their receptors (Mandell et al., 1998a,c). The matching modes were most dense in the sequence locations

TABLE 4 Human cholinergic m_1AChR targeted peptides

Sequence	Indirect agonist effect	Modulatory effect
H-FSFQCKSINYEALGY-OH	**	***
H-FSFGVKSWQYHALGY-OH	ns	*
H-ITFTVKGLTLAAFTY-OH	ns	***
H-ISFNKCTWSFERYSL-OH	ns	*
H-FNLSVKQWNYRAYNL-OH	ns	**
H-LNYQKKQYTYAAWQF-OH	ns	ns
H-LTYGVMNYGFAAFGF-OH	ns	ns
H-LGFSVCPITLAELTY-OH	ns	ns
H-LGLGVCPINLAALTW-OH	ns	ns
H-LTWNVKTYSLHELPL-OH	ns	ns

m_1 targeted peptide average side chain pKa (■ = active, ○ = nonactive)

of the receptor's respective putative extracellular loops, especially e_2 and e_3, and sometime their N-terminal segments. Similarly, wavelet transformation of the hydrophobically transformed amino acid series of the long form, D_2 dopamine receptor suggested leading eigenvector hydrophobic mode locations in the e_2 and e_3 regions (Mandell et al., 2003), extracellular to the transmembrane regions of the putative dopamine binding site (Dal Toso et al., 1989; Kozell et al., 1994; Neve and Wiens, 1995; Woodward et al., 1994). Mode-targeted, eigenvector template-designed peptides demonstrated significant positive modulatory effects on D_2 dopamine receptor-transfected cellular function, as well as dramatically augmenting dopamine-mediated behavior in the rat brain (Mandell et al., 2003).

Christopoulos and Kenakin (2002) have reviewed allosteric mechanisms using point mutagenic and chimeric exchange studies in muscarinic receptors assessed by isotopic ligand binding and cellular function. They suggest that m_i allosteric modulators such as gallamine, alcuronium, and the bis-ammonium compounds have multiple extracellular sites of action, particularly in the sequence neighborhoods of the extracellular loops, e_2 and e_3 (Birdsall et al., 1996; Christopoulos and Kenakin, 2002; Christopoulos et al., 1998; Lee and el-Fakahany, 1991; Matsui et al., 1995). Relevant to our program designing receptor-targeted, hydrophobic mode-matched peptides, it is interesting that antibodies raised to these extracellular loop polypeptide sequences have been shown to allosterically modulate and/or activate GPCRs (abu Alla et al., 1996; Mijares et al., 1996, 2000). In addition, studies using peptide fractions and/or protease sensitive tissue extracts as well as specific peptides such as dynorphin A have demonstrated allosteric actions on GPCRs (Diaz-Arrastia et al., 1985; Heron and Schimerlik, 1984; Hu and el-Fakahany, 1993; Hu et al., 1992).

The relative paucity of known allosteric agents for GPCRs, the current lack of knowledge about their sites of action, and an absence of standard techniques for designing them (beyond the use of high through-put screening of random chemical libraries) may be explained in Christopoulos' and Kenakin's comment that "... hormone or neurotransmitter receptor allosteric sites may simply represent accessory domains normally serving structural roles and it is only with the discovery of (functionally active) exogenous ligands that recognize these domains that allosteric modulation of receptor function becomes biologically relevant ..." (Christopoulos and Kenakin, 2002).

Graphs of the wavelet plane of continuous Morlet wavelet transformations of hydrophobically transformed α-helical proteins (e.g., myoglobin and hemoglobin), β-sheet proteins (e.g., concancavalan A and prealbumin) and the mixed α/β-proteins (e.g., carboxypeptidase and rhodanase) portrayed the hydrophobic mode lengths (mother wavelet scales) and sequence locations of their primary and secondary structures (Mandell et al., 1997a,b). We can bring proteins' hydrophobic wavelengths and those wavelength densities sequence locations into clearer focus by linear decomposition of their hydrophobically transformed protein sequences' lagged autocovariance matrices, and studying their leading eigenvector-generated autocovariance eigenfunctions using continuous Morlet wavelet transformation (Mandell et al., 1997b). This sequence of transformations when applied to the generic and historically best structurally characterized transmembrane receptor, rhodopsin, located the seven transmembrane segments in the amino acid sequence quite well (Mandell et al., 1997b). Subsequent wavelet transformation studies of proteins by others have confirmed the usefulness of wavelet transformations in the characterization and localization of transmembrane segments, hydrophobic cores in globular proteins, and repeating motifs (Hirakawa et al., 1999; Lio and Vannucci, 2000; Murray et al., 2002; Wouters et al., 2000).

Continuous Morlet wavelet transformations of m_1AChR's $\psi_1\,\omega^{-1} = 73.15$ aa, $\psi_2\,\omega^{-1} = 7.78$ aa, and $\psi_4\,\omega^{-1} = 2.42$ aa, as defined above, were undertaken using standard algorithms (Daubechies, 1992; Farge et al., 1993; Mallat, 1989; Strang, 1993; Wickerhauser, 1994). Generally, a Morlet wavelet transform, $T(a,b)$, of a series of n eigenfunction values, $\psi_i(n)$, consists of decomposing the series into translated, $f(n) \rightarrow f(n-b)$ and scaled, $f(n) \rightarrow f(n)/a$ (scale is analogous to the inverse radian frequency of a trigonometric function) versions of the mother Morlet wavelet, w. w is the continuous, symmetric, infinitely regular, modulated Gaussian Morlet wavelet (Grossman and Morlet, 1984) $w(n) = 1/\sqrt{2\pi}\exp(-n^2/2)\exp(2\pi ifn)$, and is composed with the data series $\psi_i(n)$as: $T(a,b) = 1/\sqrt{a}\int_0^n \psi_i(n)\, w(n-b/a)dn$.

Fig. 3, *A–C*, show the wavelet transformations of the series of the indicated leading m_1 eigenfunction. Sequence position of the wavelet coefficients is graphed along the x axis and the relative wavelength scale is plotted along the y axis. Empirically, the indicated scale divided by a little over 4 at the bottom, with the denominator decreasing toward just over 2 at the top approximating the hydrophobic (mother

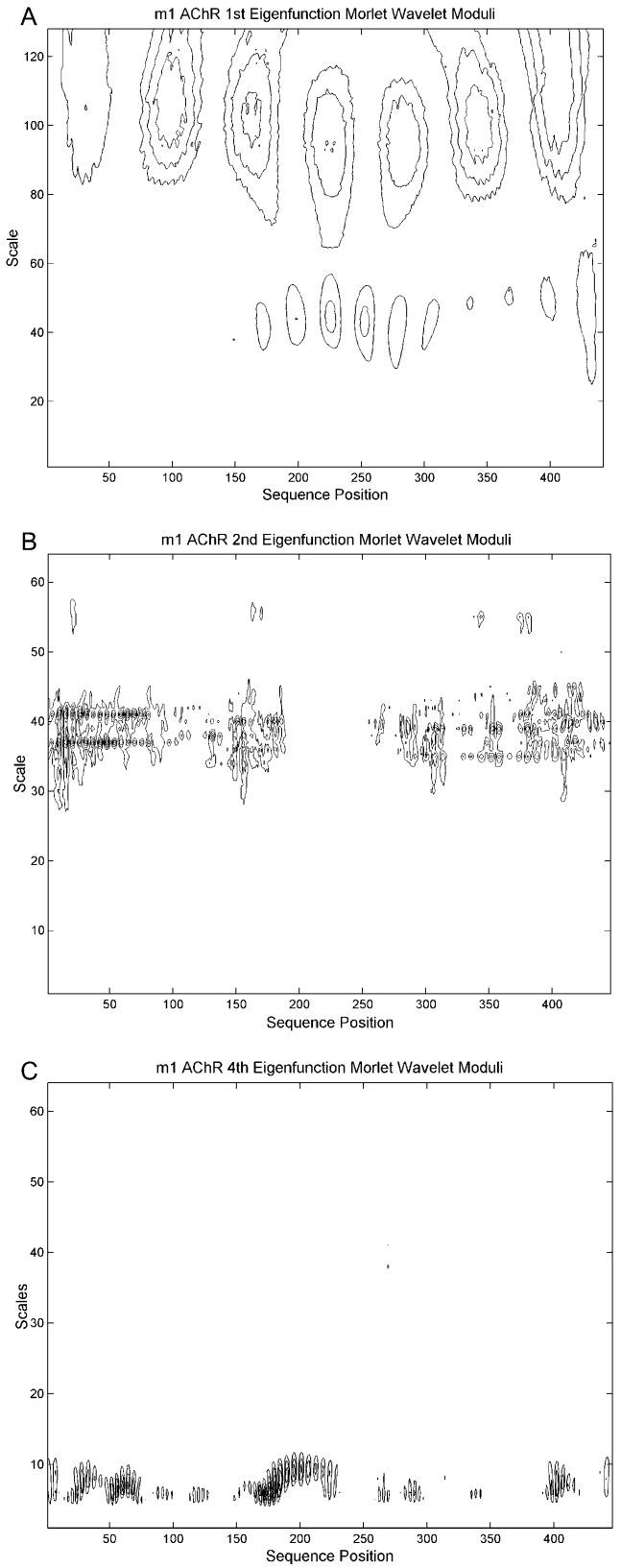

FIGURE 3 (*A–C*) Isopotential plots of the Morlet continuous one-dimensional wavelet transformation moduli of the indicated leading m_1AChR eigenfunctions. Sequence position of the wavelet coefficients is indicated along the *x* axis and the relative wavelength scale is plotted along the *y* axis. We approximate the hydrophobic (mother Morlet wavelet) eigenfunction wavelength empirically (see text). *A* graphs the continuous Morlet wavelet transformation of ψ_1, suggesting modular peaks corresponding to m_1AChR's seven transmembrane segments. *B* is a graph of the Morlet wavelet transformation of ψ_2. Densities approximate a mother wavelet wavelength corresponding to a hydrophobic wavelength of ≈7–8 aa and overlap the putative sequence locations of the N-terminal segment, e_1 (≈75–100), e_2 (≈155–180), and e_3 (≈380–405). These are proposed allosteric sites in GPCRs in general and m_1AChR in particular, and the locations we have suggested as potential peptide hydrophobic mode-matched interaction sites. *C* is a graph of the Morlet wavelet transformation of ψ_4, with a particularly prominent density at a wavelength of ≈2.5 aa, overlapping the hypothesized sequence position of the e_2 extracellular loop. It appears that the dominant sequence locations of the eigenvector modes of ψ_2 and ψ_4 are consistent with putative m_1AChR allosteric sites in the literature.

Morlet wavelet) eigenfunction wavelength (Mandell et al., 2001, 1997b,c, 1998b). The densities of the implicit *z* axis portray the modular amplitude of the wavelet transformation at the indicated scale and location, graphed in threshold isopotential plots. Fig. 3 *A* is a graph of the continuous Morlet wavelet transformation of ψ_1, suggesting modular peaks corresponding to m_1AChR's seven transmembrane segments. Fig. 3 *B* is a graph of the Morlet wavelet transformation of ψ_2, with densities approximating a mother wavelet wavelength corresponding to a hydrophobic wavelength of ≈7–8 aa, and which overlaps the putative sequence locations of the N-terminal segment, e_1 (≈75–100), e_2 (≈155–180), and e_3 (≈380–405) (SWISS-PROT, Version 41.19). This suggests, as reviewed above, the potential for peptide hydrophobic mode matched interaction at these speculated allosteric sites in GPCRs in general and m_1AChR in particular. Of course, the leading hydrophobic eigenvector containing subsequences may be part of the transmembrane receptor's structural domains, assuming the role of allosteric site only with experimentally demonstrable hydrophobic mode matched modulatory actions (Christopoulos and Kenakin, 2002) (see below). Fig. 3 *C* is a graph of the Morlet wavelet transformation of ψ_4, with a particularly prominent modular density at a wavelength of ≈2.5 aa, and overlapping the hypothesized sequence position of the e_2 extracellular loop. It appears that the dominant sequence locations of the eigenvector modes of ψ_2 and ψ_4 are not inconsistent with putative m_1AChR allosteric sites in the research reviewed above. As in these other studies, we have found that the correspondence is only approximate between the eigenvector-eigenfunction wavelengths as reflected in their power spectral compared to the mother wavelet scale transformations (Mandell et al., 2001, 1997a,b,c).

Evaluation of eigenvector hydrophobic mode matched peptides using a functional assay in m_1AChR-transfected CHO cells: the extracellular acidification rate reflection of peptide modification of muscarinic ligand-induced cellular activity.

We conduct initial testing of eigenvector template design peptides using indices of in vitro cellular and/or in vivo physiological function before further studies of the effects of

the most promising peptide on second messenger responses and radioligand binding. This is consistent with the position that ''...the current emphasis is away from radioligand binding, toward ... functional screening ...'' for allosteric ligands (Christopoulos and Kenakin, 2002). For example, we screened peptides targeting the leading autocovariance eigenmodes of the human long form D_2 dopamine receptor using microphysiometer monitored (McConnell et al., 1992) integrated extracellular acidification responses (IEAR) of stably receptor transfected CHO and mouse fibroblast LtK cells. Those peptides that produced statistically significant augmentation in this functional assay system were studied more thoroughly in a concentration-response protocol using the same assay system. Of these, the most robustly active peptides were examined in vivo, where they activated dopamine-like brain-behavioral responses in the rat (Mandell et al., 2003). Now, in our second group of studies with these peptides, we are exploring their facilitation of the dopamine-induced inhibition of forskolin-induced cAMP production in receptor-transfected LtK cells (R. Caceda, B. Kinkead, A. Mandell, K. Selz, M. Shlesinger, and M. Owens, in preparation).

The following are similar, initial studies of the modulatory effects of the peptides listed in Table 4 on muscarinic ligand-induced changes in IEAR. Data is measured microphysiometrically during the ''off'' times of the pump cycles after the indicated carbachol alone versus peptide plus carbachol exposures in m_1AChR-transfected CHO-K1 cells. The results of the experiments reported here will be followed in later studies by the development of more specific activity measures, involving radioligand binding and second messenger involved response measures (e.g., suppression of forskolin-stimulated cAMP production in muscarinic receptor transfected cell systems) (Griffin et al., 2003). It should be noted that high correlations have been reported between microphysiometric responses to muscarinic agonists and antagonists in muscarinic receptor transfected cell systems and induced changes in radioligand binding (Wood et al., 1999), Ca^{2+} mobilization measured using a fluorescent Ca^{2+} ligand (Ikeda et al., 1999), and phosphoinositide hydrolysis (Baxter et al., 1994). Nonetheless, the results of the following microphysiometric surveys of eigenvector template-generated peptide influences on receptor-mediated function in m_1AChR and m_2AChR transfected CHO-K1 cells (Kuo et al., 1993) are to be considered preliminary, awaiting the results of further studies of less ''downstream'' indices of second messenger responses.

As reported in the following section, the specificity of the actions of the eigenvector template peptides is addressed microphysiometrically and in two ways: a), within receptor families, specificity is suggested by evidence that m_1-targeted, functionally active peptides do not influence the activity of hydrophobic-mode-differing (Table 3) m_2-transfected CHO IEAR (see below); and b), across receptor families, specificity is indicated by studies showing that D_2DAR-targeted and active peptides fail to act on the m_1 stably transfected CHO-K1 cell system. Additionally, m_1AChR-targeted and active peptides fail to show functional activity in human D_2DAR stably transfected LtK or CHO cell systems (Mandell et al., 2003, and see below).

The stably m_1AChR and m_2AChR transfected Chinese hamster ovary, CHO-K1, cell systems and baseline muscarinic agonist-response microphysiometrically monitored IEAR functions

The stably m_1AChR and m_2AChR transfected CHO-K1 cell lines, developed in the Laboratory of Cell Biology, National Institute of Mental Health, and Laboratory of Molecular Biology, National Institute of Neurological Disorders and Stroke, have a long history of successful use in characterizing receptor-mediated agonist, antagonist, and allosteric ligand activity (Bonner, 1989; Buckley et al., 1988, 1989; Dorje et al., 1991; Ellis et al., 1991; Wess et al., 1990). The human m_1AChR and m_2AChR, cDNA stably transfected CHO-K1 cells were prepared using the calcium phosphate method (Buckley et al., 1989; Chen and Okayama, 1987). For each cell line, the coding regions of the receptor were derived from a human cDNA library and inserted into the expression vector, pcDNA3 (Invitrogen, San Diego, CA). The CHO-K1 cell lines were maintained in growth medium consisting of Dulbecco's modified Eagle's medium supplemented with 10% fetal calf serum, 1000 units each of penicillin G and streptomycin, and 2 mM glutamine. Except for the overnight transfection, cells were incubated in a humidified incubator at 37° and 5% CO_2. The selection media contained 250 μg/ml of geneticin.

Muscarinic cholinergic ligand-(carbachol and/or oxotremorine) induced changes in the m_1 and m_2 CHO-K1 cells' IEAR, in the presence and absence of eigenvector template-designed peptides, were determined using well-established microphysiometric functional screening methods for m_1, m_2, and other muscarinic receptor transfected cell lines (Baxter et al., 1994; Ikeda et al., 1999; Kuo et al., 1993; McConnell et al., 1992). Receptor-mediated changes in overall cellular glycolytic and respiratory metabolism and/or cellular membrane Na^+/H^+ exchanges indicate receptor-mediated cellular activation, and are reflected in changes in extracellular protonic ($[H^+]$) concentrations (McConnell et al., 1992). $[H^+]$ neutralizes the charge on the surface of the silicon oxide, photocurrent-driven semiconductor sensor and reduces the potential-driven current conductance at a rate linearly related to the rate of extracellular $[H^+]$ production. That is, $-d\mu V/dt = (+)d[H^+]/dt$.

For typical experiments, capsule cups containing from 1.5 or 2.5×10^5 cells were placed in the sensor chambers and perfused with low buffering Dulbecco's modified Eagle's medium with culture grade 0.1% bovine serum albumin at a pump rate approximating 200 μl/min. This cell number was chosen, stabilizing the baseline timed signal at $\approx$150

μV/s, empirically optimizing the trade-off between receptor-mediated cellular response sensitivity and preparation stability (i.e., avoiding cell damage secondary to excessive acid buildup in the ''pump off'' ligand exposure periods). The 2-min pump cycle consisted of a 30-s off period, allowing measurable rates of decrease in current, the conductance linearly correlated with rates of extracellular [H^+] production. This was followed by a 60 or 40 s washout, respectively, with 200 μl/min flow across the cells in a 1.4 μl volume capsule. After stabilization of the baseline extracellular acidification rates, half of the chambers were exposed to eigenvector template-designed peptides in medium for 12 min (six 2-min cycles) whereas the remaining chambers received only medium. All chambers were then exposed for 80 s to freshly prepared carbachol, 1 μM/L (approximating its EC_{50} in the m_1AChR-transfected CHO system). After a 30-min drug-free perfusion period, allowing a return to the baseline extracellular acidification rates, the procedure was repeated with the conditions in each chamber reversed. In this way, each capsule cup/chamber/pump system served as its own control. We have found that individual sample chambers can be treated multiple times over a 6–8 h period without significant degradation or drift.

Fig. 4 is a graph of the mean and standard errors of the carbachol concentration-response curves from two typical data sets from IEAR data sets, $n = 4$/ per point. Again, these represent [H^+] collection during off times of the pump cycles. The two curves differ by 10 s in time of stably m_1AChR-transfected CHO-K1 cell line exposure to the muscarinic ligand. As noted above, preliminary experiments have indicated that the carbachol EC_{50} in this preparation is $\sim 10^{-6}$ M. The sigmoid IEAR functions to carbachol (observed also after the muscarinic agent, oxotremorine, at its EC_{50} of 500 nM in this preparation, not shown) and the expected amplitude response to changing time of exposure are consistent with expectations.

The ''box-and-whiskers'' plot in Fig. 5 represents the results of studies in the above-described receptor-transfected cell system demonstrating the anticipated microphysiometric results of blocking carbachol-induced receptor-mediated actions by atropine, 250 nM. This is the concentration of atropine used in previous studies of muscarinic receptor binding assays (Owens et al., 1997). It antagonized the 1.1 μM carbachol-induced increase in IEAR response compared with untreated control levels. This inhibition was reversed by 1 h of washout by perfusion of medium alone and re-exposure to 1.1 μM carbachol. In Fig. 5, the horizontal line within each box represents median values, the vertical borders of the box represent the 25th and 75th percentiles, and the lower and upper horizontal bounds of the ''whiskers'' encompass the entire range of observed values, $n = 7$ per point.

Fig. 6 is a graph of the carbachol IEAR concentration-response functions in the stably m_2AChR transfected CHO-K1 cells line at three levels of cell number per capsule cup, $\approx$1.25, 1.50, and 2.50 $\times$ 10^5, respectively. Mean and standard errors are shown, $n = 8$ or 14 per point. The figure demonstrates the expected amplitude sensitivity to increas-

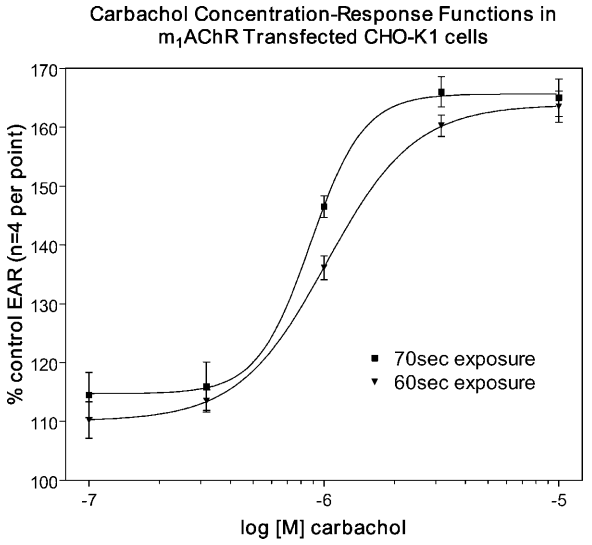

FIGURE 4 Mean and standard errors of the carbachol concentration-response curves from two typical integrated extracellular acidification responses, IEAR, data sets, $n = 4$ per point. [H^+] is collected during off times of the microphysiometer pump cycles. The top curve results from the exposure of a stably m_1AChR transfected CHO-K1 cell line to the muscarinic ligand carbachol for 70 s. The bottom curve results from a 60-s exposure time in the same system. Experiments have shown the carbachol EC_{50} in this system to be $\approx 10^{-6}$ M. The expected sigmoidal IEAR functions to carbachol and an appropriate amplitude response to changing time of exposure is demonstrated. Similar observations were made after the introduction of the muscarinic agent, oxytremorine, at EC_{50} ($\approx$500 nM) in this preparation.

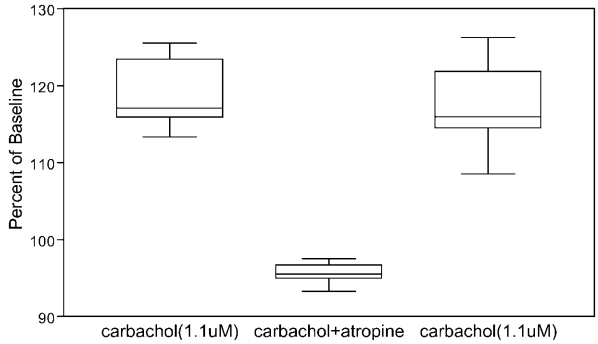

FIGURE 5 ''Box-and-whiskers'' plot showing the results of studies in a human m_1AChR stably transfected CHO-K1 cell system, demonstrating the anticipated microphysiometric results of blocking carbachol-induced receptor-mediated actions by 250 nM atropine. This is the concentration of atropine used in previous studies of muscarinic receptor binding assays (see text). The 1.1 μM carbachol-induced increase in IEAR, compared with untreated control levels, was antagonized by atropine. This inhibition was then reversed by a 1-h perfusion washout with medium alone and re-exposure to 1.1 μM carbachol, $n = 7$ per point. The horizontal line within each box represents the median value, the vertical borders of the box represent the 25th and 75th percentiles, and the lower and upper bounds of the ''whiskers'' demarcate the range of observed values.

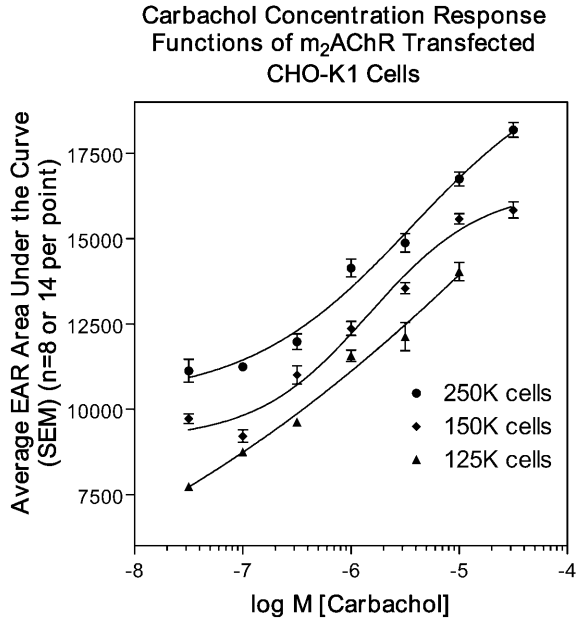

FIGURE 6 Carbachol IEAR concentration-response functions in the stably m_2AChR transfected CHO-K1 cell line at three levels of cell number per capsule cup, ≈1.25, 1.50, and 2.50 × 10^5, respectively. Mean and standard errors are shown, $n = 8$ or 14 per point. The figure demonstrates the expected amplitude sensitivity to increasing receptor-transfected cell number. All three functions manifest the same approximate EC_{50} and similar carbachol-induced, concentration-response forms.

ing receptor transfected cell numbers. All three functions manifest the same approximate EC_{50}, and similar carbachol-induced, quasisigmoid concentration-response forms. The observed ''cooperative'' sigmoid shape of the functions are expected in GPCR-mediated functional activity with the potential for allosteric interactions, allosteric here meaning the engagement of the ligand at some site in the receptor ''other'' than the orthosteric, active site (Christopoulos and Kenakin, 2002; Hall, 2000).

Muscarinic cholinergic GPCRs with the potential for allosteric regulation can be influenced at receptor-active-orthosteric (carbachol) sites, receptor-G-protein coupling sites, and receptor-allosteric sites (Christopoulos and Kenakin, 2002; Christopoulos et al., 1998; Hall, 2000). The discovery and targeting of the latter is the general goal of our algorithmic design program. As noted above, receptor-allosteric sites may be no more than an ''... accessory domain normally serving structural roles ... it is only with the discovery of exogenous ligands that recognize these domains that allosteric modulation of receptor function becomes biologically relevant ....''

Screening hydrophobic eigenvector-designed peptides for modulatory influences on carbachol-induced changes in m_1AChR-transfected CHO cells' IEAR

Table 4 (*top*) summarizes the results of a multitude of experiments screening m_1AChR-targeted peptides for indirect agonist/antagonist effects and for their capacities to modify the effects of carbachol on human m_1AChR-transfected CHO-K1 cells. Indirect agonist effects are examined as 10^{-6} M peptide in buffer versus buffer alone. Modulatory effects are evaluated using 10^{-6} M peptide plus 10^{-6} M carbachol compared with the effect of 10^{-6} M carbachol alone. $N = 8$ pairs per comparison, and ns (i.e., not significant) $\equiv p > 0.05$; * $\equiv 0.05 \geq p > 0.01$; ** $\equiv 0.01 \geq p > 0.001$; and *** $\equiv p < 0.001$. Whereas only one of the peptides (FSFQ...) acted as an indirect agonist, 5 of the 10 (FSFQ..., FSFG..., ITFT..., ISFN..., and FNLS...) demonstrated 1 μM peptide-induced augmentation of the m_1AChR-mediated, 1 μM carbachol-evoked increase in integrated $[H^+]$ production rates.

Small Kolmogorov-Smirnov distances in the data distributions (computed but not shown) justified the assumption of distributional normality and the use of *t*-tests of statistical significances of the observed differences in the data (Hoel, 1971). Recall that the integration of the rates of decrement in potential in microvolts over the off/collection portions of the pump cycles are linearly related to the rate of increment in $[H^+]$.

Table 4 (*bottom*) is a graph in which solid squares indicate physiologically active peptides and open circles signify peptides that showed no significant activity in Table 4 (*top*). Their order is dictated by their mean amino acid side-chain pKas. The physiologically inactive LNYQ..., containing two basic lysines, is represented by the open circle to the right of the diagram (*bottom*). The four more acidic inactive peptides are represented by open circles on the left of the diagram. Of the peptides in Table 4 (*top*), the eigenvector template-designed peptides with mean amino acid side-chain pKa values of between 7.4 and 7.9 were statistically significantly active, whereas peptides with mean amino acid pKas outside that range were not. A definitive statement concerning the role of average side-chain pKa values on the efficacy of eigenvector template-designed peptides in the muscarinic and other systems has yet to be systematically addressed. However, it is known that proteins as polyampholytes manifest anisotropic charge distributions such that macromolecularly local pH values can differ from that of the global assay system, and that this local variability can play a role in intermolecular recognition (Daune, 1998).

To estimate the relative probability of the de novo peptide results in Table 4, we compare our findings with the results of random and permutative peptide library searches. We assume that high through-put screening of a 200,000–300,000 component random peptide library may be expected to generated 2–4 ''hits'' (Guner, 1999; Spencer, 1998). Even using the more optimistic Bayesian prior assumption that a survey of a random peptide library would have an expectancy of as many as 5 active peptides per 100,000 candidates, i.e., $p(B) = 0.00005$, the probability of the observed rate of modulatory activity (Table 4), $p(A) = 0.5$,

would be of order $p(A|B)p(B)/p(A) = 0.000025 \times 0.0005/0.5 = 0.25 \times 10^{-8}$ (Cox and Hinkley, 1974).

Some kinetic characteristics of the modulatory actions of a representative eigenvector peptide on carbachol-induced increases in stably m_1AChR-transfected CHO-K1 cells' IEAR

Fig. 7 is a graph of the mean and standard errors for carbachol concentration-response functions at 30 nM, approximating threshold concentration of FSFQ...; $n = 4$ pairs per point, in units of averaged IEAR (i.e., integrated rates of decrement in microvolts equals integrated rates of increment in $[H^+]$). The effects of carbachol alone are compared with those of 30 nM FSFQ... plus carbachol. Again, each chamber/capsule/sensor acted as its own control. Fig. 7 demonstrates the expected peptide-induced, left-shift, and amplitude increase by a low concentration of FSFQ.... Although radioligand binding assays are considered to be the most direct way to visualize and quantify allosteric interactions with GPCRs, current GPCR allosteric theory, including that involving muscarinic receptors, suggests that functional assays can also be used to demonstrate allosteric effects (Christopoulos and Kenakin, 2002), for example, the allosteric effects of gallamine on muscarinic agonist concentration response curves in rat trachea (Kennakin and Boselli, 1989). Whereas indirect antagonism and negative cooperativity may be more difficult to demonstrate, often misinterpreted as competitive antagonism, "... in the case of (apparent) positive cooperativity, the ascription of an allosteric mechanism to the experimental data would be relatively straightforward because the agonist curves would be displaced to the left of the control agonist curve" (Christopoulos and Kenakin, 2002).

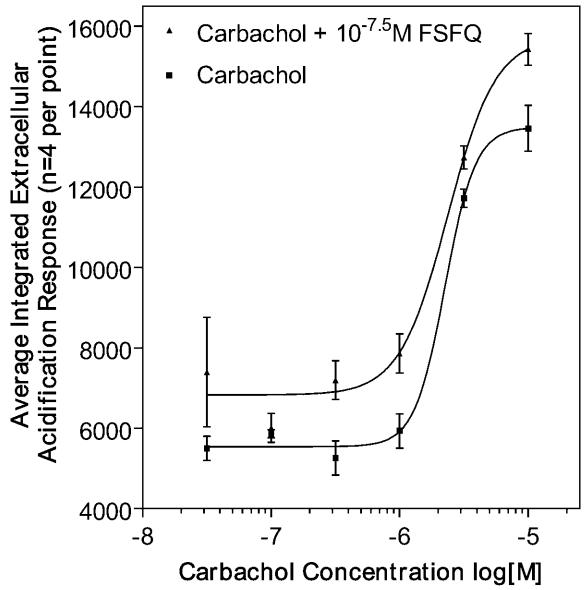

FIGURE 7 Mean and standard errors for carbachol concentration-response functions at a 30 nM, approximating the threshold concentration of FSFQ..., $n = 4$ pairs per point. The effects of carbachol alone are compared with those of 30nM FSFQ... plus carbachol in arbitrary units reflecting the relative integrated rate of extracellular proton $[H^+]$ production, measured as the inverse rate of decrement in microvolt potential. Again, each chamber/capsule/sensor acted as its own control. The figure demonstrates the expected peptide-induced, left-shift, and amplitude increase by a low concentration of FSFQ..., suggesting a positive cooperative allosteric mechanism (see text).

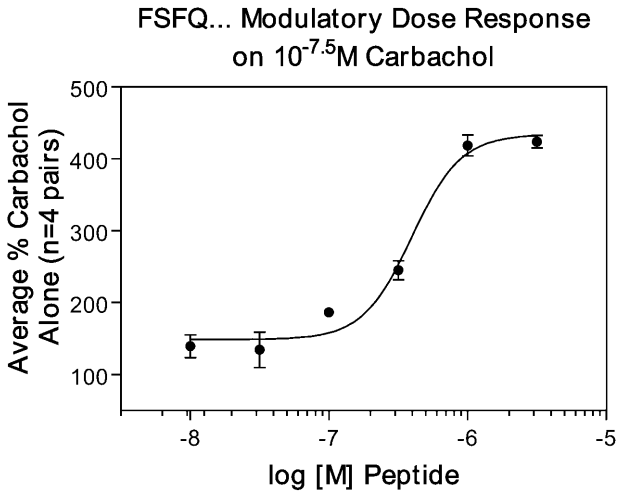

FIGURE 8 Concentration-response behavior of the putative positive allosteric influence of FSFQ.... An FSFQ... concentration-response function of the positive modulatory effect of FSFQ... plus carbachol was compared with the effect of a relatively low (30 nM) concentration of carbachol alone. Mean and standard errors of the IEAR of the FSFQ... plus carbachol condition are represented as a percent of the carbachol alone condition, $n = 4$ pairs per point. The asymptotic FSFQ... function is consistent with the concentration-response behavior of a positive allosteric modulator. The EC_{50} of the peptide effect ≈300 nM (see text).

Fig. 8 addresses the concentration-response behavior of the putative positive allosteric influence of FSFQ.... It shows the mean and standard errors of the IEAR of an FSFQ... concentration-response function of the positive modulatory effect of FSFQ... plus carbachol compared with the effect of a relatively low (30 nM) concentration of carbachol alone, $n = 4$ pairs per point. This asymptotic peptide ligand-induced sigmoid function is consistent with the concentration-response behavior of a positive allosteric modulator of muscarinic and other GPCRs (Christopoulos and Kenakin, 2002; Hall, 2000). These results suggest

TABLE 5 Normalized difference in carbachol versus carbachol + peptide hill slopes across FSFQ... concentrations

[FSFQ...]	$(HS_{C+P} - HS_C)/HS_C$
10 nM	−7029
30 nM	−3707
100 nM	.4054
300 nM	1.3536
1 μM	3.5696
3 μM	1.2511

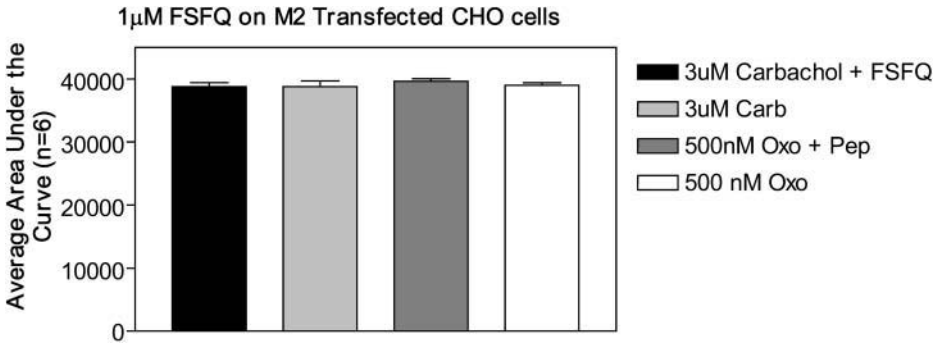

FIGURE 9 IEAR of the muscarinic agonists, 3 μM carbachol or 500 nM oxotremorine, on stably m_2AChR transfected CHO cells. Both agonists were tested at their approximate EC_{50} values in this m_2 receptor-transfected cell system, and were studied in the absence and presence of 1 μM of the m_1 receptor active FSFQ. . ., $n = 6$ for each bar. No significant peptide effects on either of the muscarinic agent-induced increases in units of IEAR in the hydrophobic eigenvector mode differing m_2 (Table 3) transfected CHO-K1 system were observed.

an allosteric EC_{50} for FSFQ. . . of ~300 nM (i.e., the concentration of peptide that produces half-maximal effect of peptide allosteric modulator (Ehlert, 1988)).

The Hill slope or Hill number, HS or n_H, is an index frequently used for quantification of the amount of kinetic cooperativity in a ligand/receptor system. It is an exponent reflecting the slope of the part of the concentration-rate response function encompassing the middle 50% saturation region (usually studied between 10% and 90% of the maximal effect) of the ligand concentration versus response plot (Ferscht, 1985; Goldbeter and Koshland, 1981; Lauffenburger and Linderman, 1993; Limbird, 1986), and is without established physical bases (Lauffenburger and Linderman, 1993). The higher the value of HS, the greater is said to be the amount or degree of cooperativity. We compute the best-fit HS to a series of real data concentration-response functions representing the effects of the indicated range of fixed FSFQ. . . concentrations in Table 5, as examined across the range of carbachol concentrations used in the study in Fig. 7. Table 5 summarizes the results of these studies in which, as noted, the Hill slope is presented as the normalized difference in HS between the two treatment conditions, carbachol plus peptide, $C + P$, and carbachol alone, C, (i.e., $(HS_{C+P} - HS_C)/HS_C$) at increasing fixed FSFQ. . . concentrations. The real data functions were used to compute best-fit HS values as in an idealized cooperative sigmoid curve, $[C]^{HS}/1+[C]^{HS}$.

Table 5 documents a peptide-induced increase in the normalized HS difference with increasing concentration of FSFQ. . .. This is consistent with an FSFQ. . .-induced, concentration-dependent increase in cooperativity with increasing peptide levels, from 10 nM to 1 μM. Note that the normalized HS difference at higher peptide concentration approaches a no-difference asymptote at 3 μM. Here, as in Fig. 8, an estimate of the positive cooperative allosteric EC_{50} of FSFQ. . . appears to be ≈300 nM.

Two sources of evidence for GPCR-targeted, modulatory eigenvector-templated peptide hydrophobic eigenvector mode specificity

"Within family" comparisons of peptide actions on m_1AChR- versus m_2AChR-mediated cellular activity

We employed the same microphysiometric protocol described above, with ≈2.5×10^5 m_2AChR-transfected CHO-K1 cells per capsule cup. Recall that m_1AChR and m_2AChR differed in their dominant hydrophobic eigenmodes (Table

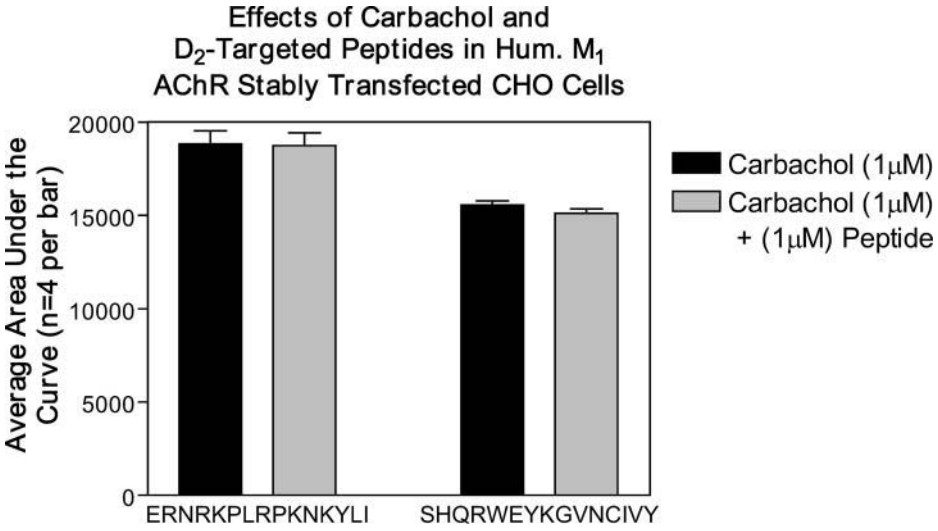

FIGURE 10 Previous algorithmic peptide design studies targeting the human long form D_2 dopamine receptor, D_2DAR, have shown the peptides ERNR. . . and SHQR. . . to be robust indirect agonist and/or positive allosteric modulators of dopamine-induced increases in the IEAR in D_2DAR-transfec as distributionally weighted LtK and CHO cell systems (Mandell et al., 2003). The hydrophobic eigenmodes of the dopamine D_2DAR are distinct from those of the m_1AChR. Neither 1 μM ERNR. . . nor 1 μM SHQR. . . had significant effects on the 1 μM carbachol activation of the m_1AChR-transfected CHO-K1 cells.

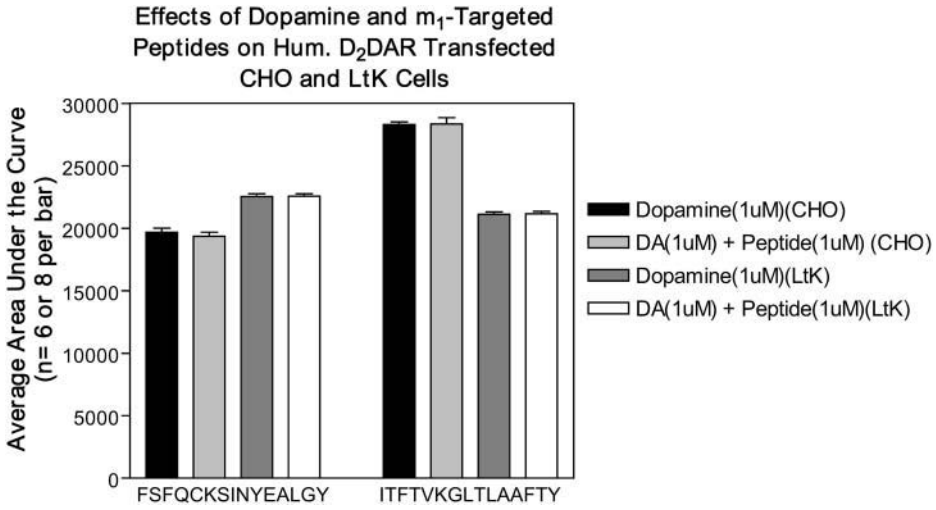

FIGURE 11 Mean and standard errors of the effects of 1 μM of m_1AChR-targeted, active peptides FSFQ... and ITFT... on D_2DAR-transfected CHO-K1 and LtK cells. Neither of the m_1AChR-targeted de novo peptides produced statistically significant modulatory effects on 1 μM dopamine-induced increases in IEAR in either cell system; $n = 6$ or 8 per bar.

3). Fig. 9 is a graph of the results of these experiments, in which the muscarinic agonists, 3 μM carbachol or 500 nM oxotremorine (both at their approximate EC_{50}s in this m_2 receptor-transfected cell system) were studied in the absence and presence of 1 μM of the m_1 receptor active FSFQ..., $n = 6$ for each bar. No significant peptide effects on either of the muscarinic agent-induced increases in units of IEAR in the hydrophobic eigenvector mode differing m_2 (Table 3) transfected CHO-K1 system were observed. This finding is consistent with our hypothesis that hydrophobic autocovariance eigenvector mode specificity *within* the muscarinic receptor family appears to be of physiological significance with respect to peptide-receptor signaling.

"Across family" comparisons of D_2 dopamine receptor, D_2DAR, active eigenvector peptide actions on m1AChR-transfected CHO-K1 cells and m1AChR active eigenvector peptides on D_2DAR-transfected CHO-K1 and (mouse fibroblast) LtK cells

In previous algorithmic peptide design studies targeting the human long form D_2 dopamine receptor, ERNR... and SHQR... were among the strongest indirect agonist and/or positive allosteric modulators of dopamine-induced increases in the IEAR in D_2DAR-transfected LtK and CHO cell systems (Mandell et al., 2003). Their retro-inverso analogs (containing the same eigenvector modes as ERNR... and SHQR...), when administered bilaterally in 0.5 nmol into rats' nucleus accumbens, generated both amphetamine-like increases in exploratory behavior and reductions of prepulse inhibition (Mandell et al., 2003). Note that neither 1 μM ERNR... nor 1 μM SHQR... had significant effects on the 1 μM carbachol activation of the m_1AChR-transfected CHO-K1 cells (Fig. 10).

Fig. 11, in studies of the inverse condition to that of Fig. 10, shows the effects of 1 μM of m_1AChR-targeted and active peptides, FSFQ... or ITFT... on D_2DAR-transfected CHO-K1 and LtK cells. Neither m_1AChR targeted de novo peptide produced statistically significant modulatory effects on 1 μM dopamine-induced increases in IEAR in either cell system, $n = 6$ or 8 per bar.

In the context of mode specificity, it is important to recall precisely which mode representation is being discussed. It is the leading hydrophobic autocovariance matrix eigenvector(s) (as in Fig. 2 *E*), and not the statistical wavelength approximations by their eigenvector/eigenfunction's maximum entropy power spectra (as in Fig. 2, *B* and *D*), that most specifically represent what we regard as the operative signaling hydrophobic modes. Given this, the findings of across D_2DAR and m_1AChR families comparison of Figs. 10 and 11 (Mandell et al., 2003), along with the m_1AChR versus m_2AChR within receptor family comparisons of Table 3 and Fig. 9, are consistent with our hypothesis that hydrophobic eigenvector mode-matching specificity can play an important role in peptide-receptor signaling (Mandell et al., 1997c).

Appreciation is expressed to Prof. Alan Levey, Department of Neurology, Emory University School of Medicine, for the initial gift of transfected cell lines and technical consultation. The authors express thanks to the reviewers for their informed and constructive comments.

This work was supported in part by grants to A.J.M. and K.A.S. from the National Institute of Mental Health (58026) and the National Cancer Institute (91384). M.J.O. receives grant and consultancy support and honoraria from Cielo Institute, National Alliance for Research on Schizophrenia and Depression, National Institutes of Health, Forest Labs, Merck, Pfizer, Glaxo SmithKline, Cypress Biosciences, and Bristol Myers-Squibb.

REFERENCES

abu Alla, S., U. Quitterer, S. Grigoriev, A. Maidhof, M. Haasemann, K. Jarnagin, and W. Muller-Esterl. 1996. Extracellular domains of the bradykinin B_2 receptor involved in ligand binding and agonist sensing defined by anti-peptide antibodies. *J. Biol. Chem.* 271:1748–1755.

Adem, A., M. Jolkkonen, N. Bogdanovic, A. Islam, and E. Karlsson. 1997. Localization of M1 muscarinic receptors in rat brain using selective muscarinic toxin-1. *Brain Res. Bull.* 44:597–601.

Adem, A., and E. Karlsson. 1997. Muscarinic receptor subtype selective toxins. *Life Sci.* 60:1069–1076.

Anfinsen, C. B. 1973. Principles that govern the folding of protein chains. *Science.* 181:223–230.

Bartus, R. T., R. L. Dean 3rd, B. Beer, and A. S. Lippa. 1982. The cholinergic hypothesis of geriatric memory dysfunction. *Science.* 217:408–414.

Bashford, D., and D. A. Case. 2000. Generalized born models of macromolecular solvation effects. *Annu. Rev. Phys. Chem.* 51:129–152.

Baxter, G. T., M. L. Young, D. L. Miller, and J. C. Owicki. 1994. Using microphysiometry to study the pharmacology of exogenously expressed m1 and m3 muscarinic receptors. *Life Sci.* 55:573–583.

Beattie, J., J. H. Shand, C. Burns, and D. J. Flint. 1996a. Immunodominant regions of the extra-cellular domain of the bovine growth hormone receptor. *Biochem. Soc. Trans.* 24:307S.

Beattie, J., J. H. Shand, and D. J. Flint. 1996b. An immobilised peptide array identifies antibodies to a discontinuous epitope in the extracellular domain of the bovine growth hormone receptor. *Eur. J. Biochem.* 239:479–486.

Bendat, J. S. 1958. Principles and Applications of Random Noise Theory. John Wiley & Sons, New York.

Bendat, J. S., and A. G. Piersol. 1986. Random Data; Analysis and Measurement Procedures. Wiley-Interscience, New York.

Ben-Naim, A. 1980. Hydrophobic Interactions. Plenum, New York.

Birdsall, N. J., F. Cohen, S. Lazareno, and H. Matsui. 1995. Allosteric regulation of G-protein-linked receptors. *Biochem. Soc. Trans.* 23:108–111.

Birdsall, N. J., T. Farries, P. Gharagozloo, S. Kobayashi, D. Kuonen, S. Lazareno, A. Popham, and M. Sugimoto. 1997. Selective allosteric enhancement of the binding and actions of acetylcholine at muscarinic receptor subtypes. *Life Sci.* 60:1047–1052.

Birdsall, N. J., E. C. Hulme, and J. M. Stockton. 1983. Muscarinic receptor subclasses: allosteric interactions. *Cold Spring Harb. Symp. Quant. Biol.* 48:53–56.

Birdsall, N. J., S. Lazareno, and H. Matsui. 1996. Allosteric regulation of muscarinic receptors. *Prog. Brain Res.* 109:147–151.

Blanc, J. P., J. W. Taylor, R. J. Miller, and E. T. Kaiser. 1983. Examination of the requirement for an amphiphilic helical structure in beta-endorphin through the design, synthesis, and study of model peptides. *J. Biol. Chem.* 258:8277–8284.

Bohm, H.-J., and G. Klebe. 1996. What can we learn from molecular recognition in protein-ligand complexes for the design of new drugs? *Angew Chem. Int. Ed. Engl.* 35:2588–2614.

Bonner, T. I. 1989. New subtypes of muscarinic acetylcholine receptors. *Trends Pharmacol. Sci.* Suppl: 11–15.

Bonner, T. I., N. J. Buckley, A. C. Young, and M. R. Brann. 1987. Identification of a family of muscarinic acetylcholine receptor genes. *Science.* 237:527–532.

Box, G. E. P., and G. M. Jenkins. 1970. Time Series Analysis, Forecasting and Control. Holden-Day, San Francisco.

Branden, C., and J. Tooze. 1999. Introduction to Protein Structure, 2nd ed. Garland, New York.

Brillinger, D. 1981. Time Series: Data Analysis and Theory. Holden-Day, New York.

Broomhead, D. S., R. Jones, and G. P. King. 1987. Addenda and correction. *J. Phys. A.* 20:L563–L569.

Broomhead, D. S., and G. P. King. 1986. Extracting qualitative dynamics from experimental data. *Physica D.* 20:217–236.

Bruccoleri, R. E., E. Haber, and J. Novotny. 1988. Structure of antibody hypervariable loops reproduced by a conformational search algorithm. *Nature.* 335:564–568.

Buck, K. J., and S. G. Amara. 1995. Structural domains of catecholamine transporter chimeras involved in selective inhibition by antidepressants and psychomotor stimulants. *Mol. Pharmacol.* 48:1030–1037.

Buckley, N. J., T. I. Bonner, and M. R. Brann. 1988. Localization of a family of muscarinic receptor mRNAs in rat brain. *J. Neurosci.* 8:4646–4652.

Buckley, N. J., T. I. Bonner, C. M. Buckley, and M. R. Brann. 1989. Antagonist binding properties of five cloned muscarinic receptors expressed in CHO-K1 cells. *Mol. Pharmacol.* 35:469–476.

Caflisch, A., and M. Karplus. 1994. Molecular dynamics simulation of protein denaturation: solvation of the hydrophobic cores and secondary structure of barnase. *Proc. Natl. Acad. Sci. USA.* 91:1746–1750.

Chalaskinski, G., and M. M. Szczesniak. 1994. Origins of structure and energetics of van der Waals cluster from ab initio calculations. *Chem. Rev.* 94:1723–1765.

Chen, C. J., and H. Okayama. 1987. High efficiency transformation of mammalian cells by plasmid DNA. *Mol. Cell. Biol.* 7:2745–2752.

Chothia, C. 1974. Hydrophobic bonding and accessible surface area in proteins. *Nature.* 248:338–339.

Chothia, C. 1975. Structural invariants in protein folding. *Nature.* 254:304–308.

Chothia, C., and J. Janin. 1975. Principles of protein-protein recognition. *Nature.* 256:705–708.

Chou, P. Y., and G. D. Fasman. 1974a. Conformational parameters for amino acids in helical, beta-sheet, and random coil regions calculated from proteins. *Biochemistry.* 13:211–222.

Chou, P. Y., and G. D. Fasman. 1974b. Prediction of protein conformation. *Biochemistry.* 13:222–245.

Christopoulos, A., and T. Kenakin. 2002. G protein-coupled receptor allosterisms and complexing. *Pharmacol. Rev.* 54:323–374.

Christopoulos, A., A. Lanzafame, and F. Mitchelson. 1998. Allosteric interactions at muscarinic cholinoceptors. *Clin. Exp. Pharmacol. Physiol.* 25:185–194.

Cornette, J. L., K. B. Cease, H. Margalit, J. L. Spouge, J. A. Berzofsky, and C. DeLisi. 1987. Hydrophobicity scales and computational techniques for detecting amphipathic structures in proteins. *J. Mol. Biol.* 195:659–685.

Cox, D. R., and D. V. Hinkley. 1974. Theoretical Statistics. Chapman and Hall, London.

Creighton, T. 1993. Proteins: Structures and Molecular Properties, 2nd ed. W. H. Freeman, New York.

Dal Toso, R., B. Sommer, M. Ewert, A. Herb, D. B. Pritchett, A. Bach, B. D. Shivers, and P. H. Seeburg. 1989. The dopamine D2 receptor: two molecular forms generated by alternative splicing. *EMBO J.* 8:4025–4034.

Damasio, A. R., N. R. Graff-Radford, P. J. Eslinger, H. Damasio, and N. Kassell. 1985. Amnesia following basal forebrain lesions. *Arch. Neurol.* 42:263–271.

Daubechies, I. 1992. Ten Lectures on Wavelets. SIAM, Philadelphia.

Daune, M. 1998. Molecular Biophysics. Oxford University Press, Oxford.

Davis, K. L., L. J. Thal, E. R. Gamzu, C. S. Davis, R. F. Woolson, S. I. Gracon, D. A. Drachman, L. S. Schneider, P. J. Whitehouse, and T. M. Hoover. 1992. A double-blind, placebo-controlled multicenter study of tacrine for Alzheimer's disease. *N. Engl. J. Med.* 327:1253–1259.

Deber, C. M., M. Glibowicka, and G. A. Woolley. 1990. Conformations of proline residues in membrane environments. *Biopolymers.* 29:149–157.

Diaz-Arrastia, R., T. Ashizawa, and S. H. Appel. 1985. Endogenous inhibitor of ligand binding to the muscarinic acetylcholine receptor. *J. Neurochem.* 44:622–628.

Dickinson-Anson, H., I. Aubert, F. H. Gage, and L. J. Fisher. 1998. Hippocampal grafts of acetylcholine-producing cells are sufficient to improve behavioral performance following a unilateral fimbria-fornix lesion. *Neuroscience.* 84:771–781.

Dill, K. A., S. Bromberg, K. Yue, K. M. Fiebig, D. P. Yee, P. D. Thomas, and H. S. Chan. 1995. Principles of protein folding—a perspective from simple exact models. *Protein Sci.* 4:561–602.

Dill, K. A., K. M. Fiebig, and H. S. Chan. 1993. Cooperativity in protein-folding kinetics. *Proc. Natl. Acad. Sci. USA.* 90:1942–1946.

Dorje, F., J. Wess, G. Lambrecht, R. Tacke, E. Mutschler, and M. R. Brann. 1991. Antagonist binding profiles of five cloned human huscarinic receptor subtypes. *J. Pharmacol. Exp. Ther.* 256:727–733.

Duerson, K., R. Carroll, and D. Clapham. 1993. Alpha-helical distorting substitution disrupt coupling between m3 muscarinic receptor and G proteins. *FEBS Lett.* 324:103–108.

Dunker, A. K., E. Garner, S. Guilliot, P. Romero, K. Albrecht, J. Hart, Z. Obradovic, C. Kissinger, and J. E. Villafranca. 1998. Protein disorder and the evolution of molecular recognition: theory, predictions and observations. *Pac. Symp. Biocomput.* 473–484.

Dunker, A. K., J. D. Lawson, C. J. Brown, R. M. Williams, P. Romero, J. S. Oh, C. J. Oldfield, A. M. Campen, C. M. Ratliff, K. W. Hipps, J. Ausio, M. S. Nissen, R. Reeves, C. Kang, C. R. Kissinger, R. W. Bailey, M. D. Griswold, W. Chiu, E. C. Garner, and Z. Obradovic. 2001. Intrinsically disordered protein. *J. Mol. Graph. Model.* 19:26–59.

Dunker, A. K., and Z. Obradovic. 2001. The protein trinity–linking function and disorder. *Nat. Biotechnol.* 19:805–806.

Dyson, H. J., and P. E. Wright. 2002a. Coupling of folding and binding for unstructured proteins. *Curr. Opin. Struct. Biol.* 12:54–60.

Dyson, H. J., and P. E. Wright. 2002b. Insights into the structure and dynamics of unfolded proteins from nuclear magnetic resonance. *Adv. Prot. Chem.* 62:311–340.

Edsall, J. T., and J. Wyman. 1958. Biophysical Chemistry. Academic Press, New York.

Ehlert, F. J. 1988. Estimation of the affinities of allosteric ligands using radioligand binding and pharmacological null methods. *Mol. Pharmacol.* 33:187–194.

Ehlert, F. J., and F. M. Delen. 1990. Influence of pH on the binding of scopolamine and N-methylscopolamine to muscarinic receptors in the corpus striatum and heart of rats. *Mol. Pharmacol.* 38:143–147.

Eisenberg, D., R. M. Weiss, and T. C. Terwilliger. 1984. The hydrophobic moment detects periodicity in protein hydrophobicity. *Proc. Natl. Acad. Sci. USA.* 81:140–144.

Ellis, J., J. Huyler, and M. R. Brann. 1991. Allosteric regulation of cloned m1-m5 muscarinic receptor subtypes. *Biochem. Pharmacol.* 42:1927–1932.

Farge, M., J. C. R. Hunt, and J. C. Vassilicos. 1993. Wavelets, fractals and Fourier transforms: detection and analysis of structure. *In* Wavelets, Fractals and Fourier Transforms. M. Farge, J. C. R. Hunt, and J. C. Vassilicos, editors. Clarendon Press, Oxford. 1–38.

Fauchere, J.-L., and V. Pliska. 1983. Hydrophobic parameters of pi amino acid-side chains from the partitioning of N-acetyl-amino-acid amides. *Eur. J. Med. Chem.-Chim. Ther.* 18:369–375.

Ferscht, A. 1985. Enzyme Structure and Mechanism, 2nd ed. Freeman, San Francisco.

Fetrow, J. S., J. S. Spitzer, B. M. Gilden, S. J. Mellender, T. J. Begley, B. J. Haas, and T. L. Boose. 1998. Structure, function, and temperature sensitivity of directed, random mutants at proline 76 and glycine 77 in omega-loop D of yeast iso-1-cytochrome c. *Biochemistry.* 37:2477–2487.

Fisher, L. J., H. K. Raymon, and F. H. Gage. 1993. Cells engineered to produce acetylcholine: therapeutic potential for Alzheimer's disease. *Ann. N. Y. Acad. Sci.* 695:278–284.

Flicker, C., R. Dean, R. T. Bartus, S. H. Ferris, and T. Crook. 1985. Animal and human memory dysfunctions associated with aging, cholinergic lesions, and senile dementia. *Ann. N. Y. Acad. Sci.* 444:515–517.

Franks, F. 1972. Water: A Comprehensive Treatise, Vol. 1. Plenum Press, New York.

Fraser, C. M., C. D. Wang, D. A. Robinson, J. D. Gocayne, and J. C. Venter. 1989. Site-directed mutagenesis of m1 muscarinic acetylcholine receptors: conserved aspartic acids play important roles in receptor function. *Mol. Pharmacol.* 36:840–847.

Fukunaga, K. 1990. Introduction to Statistical Pattern Recognition. Academic Press, New York.

Fukushima, D., S. Yokoyama, D. J. Kroon, F. J. Kezdy, and E. T. Kaiser. 1980. Chain length-function correlation of amphiphilic peptides. Synthesis and surface properties of a tetratetracontapeptide segment of apolipoprotein A-I. *J. Biol. Chem.* 255:10651–10657.

Gething, M.-J. 1997. Guidebook to Molecular Chaperones and Protein-Folding Catalysts. Sambrook-Tooze-Oxford, Oxford.

Gibney, B. R., Y. Isogai, F. Rabanal, K. S. Reddy, A. M. Grosset, C. C. Moser, and P. L. Dutton. 2000. Self-assembly of heme A and heme B in a designed four-helix bundle: implications for a cytochrome c oxidase maquette. *Biochemistry.* 39:11041–11049.

Giuliani, A., R. Benigni, M. Colafranceschi, I. Chandrashekar, and S. M. Cowsik. 2003. Large contact surface interactions between proteins detected by time series analysis methods: Case study on C-phycocyanins. *Proteins.* 51:299–310.

Giuliani, A., R. Benigni, P. Sirabella, J. P. Zbilut, and A. Colosimo. 2000. Nonlinear methods in the analysis of protein sequences: a case study in rubredoxins. *Biophys. J.* 78:136–149.

Giuliani, A., R. Benigni, J. P. Zbilut, C. L. Webber, Jr., P. Sirabella, and A. Colosimo. 2002. Nonlinear signal analysis methods in the elucidation of protein sequence-structure relationships. *Chem. Rev.* 102:1471–1492.

Gnagey, A. L., M. Seidenberg, and J. Ellis. 1999. Site-directed mutagenesis reveals two epitopes involved in the subtype selectivity of the allosteric interactions of gallamine at muscarinic acetylcholine receptors. *Mol. Pharmacol.* 56:1245–1253.

Godzik, A., and J. Skolnick. 1992. Sequence-structure matching in globular proteins: application to supersecondary and tertiary structure determination. *Proc. Natl. Acad. Sci. USA.* 89:12098–12102.

Goldbeter, A., and D. E. Koshland Jr. 1981. An amplified sensitivity arising from covalent modification in biological systems. *Proc. Natl. Acad. Sci. USA.* 78:6840–6844.

Golub, G. H., and C. F. Van Loan. 1993. Matrix Computations. Johns Hopkins Press, Baltimore.

Griffin, M. T., J. C. Hsu, D. Shehnaz, and F. J. Ehlert. 2003. Comparison of the pharmacological antagonism of M2 and M3 muscarinic receptors expressed in isolation and in combination. *Biochem. Pharmacol.* 65:1227–1241.

Gronenborn, A. M., and G. M. Clore. 1994. Experimental support for the ''hydrophobic zipper'' hypothesis. *Science.* 263:536.

Grossman, A., and J. Morlet. 1984. Decomposition of Hardy functions into square integrable wavelets of constant shape. *SIAM J. Math. Anal.* 15:723–736.

Guevara, M. R., L. Glass, and A. Shrier. 1981. Phase locking, period-doubling bifurcations, and irregular dynamics in periodically stimulated cardiac cells. *Science.* 214:1350–1353.

Gunasekaran, K., H. A. Nagarajaram, C. Ramakrishnan, and P. Balaram. 1998. Stereochemical punctuation marks in protein structures: glycine and proline containing helix stop signals. *J. Mol. Biol.* 275:917–932.

Guner, O. F., editor. 1999. Pharmacophore, Perception, Development and Use in Drug Design. International University Line, La Jolla, CA.

Hall, D. A. 2000. Modeling the functional effects of allosteric modulators at pharmacological receptors: an extension of the two-state model of receptor activation. *Mol. Pharmacol.* 58:1412–1423.

Heron, G. S., and M. I. Schimerlik. 1984. Protein composition of the atrial muscarinic acetylcholine receptor partially purified by wheat germ agglutinin affinity chromatography. *Arch. Biochem. Biophys.* 230:533–542.

Hirakawa, M., S. Muta, and S. Kuhara. 1999. The hydrophobic core of proteins predicted by wavelet analysis. *Bioinformatics.* 15:141–148.

Hoel, P. G. 1971. Introduction to Mathematical Statistics. Wiley, New York.

Housset, D., and J. C. Fontecilla-Camps. 1996. The structures and evolution of snake toxins of the three-finger folding type. *In* Protein Toxin Structure. M. W. Parker, editor. Springer, New York. 271–290.

Howl, J., and M. Wheatley. 1996. Molecular recognition of peptide and non-peptide ligands by the extracellular domains of neurohypophysial hormone receptors. *Biochem. J.* 317:577–582.

Hruby, V. J., and R. S. Agnes. 1999. Conformation-activity relationships of opioid peptides with selective activities at opioid receptors. *Biopolymers.* 51:391–410.

Hu, J., and E. E. el-Fakahany. 1993. Allosteric interaction of dynorphin and myelin basic protein with muscarinic receptors. *Pharmacology.* 47:351–359.

Hu, J., S. Z. Wang, C. Forray, and E. E. el-Fakahany. 1992. Complex allosteric modulation of cardiac muscarinic receptors by protamine: potential model for putative endogenous ligands. *Mol. Pharmacol.* 42:311–321.

Hulme, E. C. 1990. Muscarinic acetylcholine receptors: typical G-coupled receptors. *Symp. Soc. Exp. Biol.* 44:39–54.

Hulme, E. C., C. A. Curtis, K. M. Page, and P. G. Jones. 1995. The role of charge interactions in muscarinic agonist binding, and receptor-response coupling. *Life Sci.* 56:891–898.

Hulme, E. C., E. Kurtenbach, and C. A. Curtis. 1991. Muscarinic acetylcholine receptors: structure and function. *Biochem. Soc. Trans.* 19:133–138.

Huntly, J. J., W. Fast, S. J. Benkovic, D. C. Wright, and H. J. Dyson. 2003. Role of solvent-exposed tryptophan in the recognition and binding of antibiotic substrates for a metallo-beta-lactamase. *Protein Sci.* 12:1368–1375.

Ikeda, K., S. Kobayashi, M. Suzuki, K. Miyata, T. Yamada, and K. Honda. 1999. Ca2+ mobilization and activation of extracellular acidification by carbachol in acutely dispersed cells from guinea pig detrusor: fura 2 fluorometry and microphysiometry using the cytosensor. *Life Sci.* 65:1569–1577.

Irback, A., C. Peterson, and F. Potthast. 1996. Evidence for nonrandom hydrophobicity structures in protein chains. *Proc. Natl. Acad. Sci. USA.* 93:9533–9538.

Irback, A., and E. Sandelin. 2000. On hydrophobicity correlations in protein chains. *Biophys. J.* 79:2252–2258.

Israelachvili, J., and H. Wennerstrom. 1996. Role of hydration and water structure in biological and colloidal interactions. *Nature.* 379:219–225.

Israelachvilli, J. 1992. Intermolecular and Surface Forces, 2nd ed. Academic Press, San Diego.

Jakubik, J., L. Bacakova, E. E. El-Fakahany, and S. Tucek. 1997. Positive cooperativity of acetylcholine and other agonists with allosteric ligands on muscarinic acetylcholine receptors. *Mol. Pharmacol.* 52:172–179.

Jakubik, J., L. Bacakova, V. Lisa, E. E. el-Fakahany, and S. Tucek. 1996. Activation of muscarinic acetylcholine receptors via their allosteric binding sites. *Proc. Natl. Acad. Sci. USA.* 93:8705–8709.

Janin, J. 1995. Protein-protein recognition. *Prog. Biophys. Mol. Biol.* 64:145–166.

Jerusalinsky, D., and A. L. Harvey. 1994. Toxins from mamba venoms: small proteins with selectivities for different subtypes of muscarinic acetylcholine receptors. *Trends Pharmacol. Sci.* 15:424–430.

Jerusalinsky, D., A. Harvey, E. Karlsson, and L. Potter. 1997. Workshop: the use of muscarinic toxins in the study of muscarinic receptors. *Life Sci.* 60:1161–1162.

Jolkkonen, M., A. Adem, U. Hellman, C. Wernstedt, and E. Karlsson. 1995. A snake toxin against muscarinic acetylcholine receptors: amino acid sequence, subtype specificity and effect on guinea-pig ileum. *Toxicon.* 33:399–410.

Kaiser, E. T., and F. J. Kezdy. 1983. Secondary structures of proteins and peptides in amphiphilic environments. (A review). *Proc. Natl. Acad. Sci. USA.* 80:1137–1143.

Kamtekar, S., J. M. Schiffer, H. Xiong, J. M. Babik, and M. H. Hecht. 1993. Protein design by binary patterning of polar and nonpolar amino acids. *Science.* 262:1680–1685.

Kashihara, K., E. V. Varga, S. L. Waite, W. R. Roeske, and H. I. Yamamura. 1992. Cloning of the rat M3, M4 and M5 muscarinic acetylcholine receptor genes by the polymerase chain reaction (PCR) and the pharmacological characterization of the expressed genes. *Life Sci.* 51:955–971.

Kauzmann, W. 1959. Some factors in the interpretation of protein denaturation. *Adv. Protein Chem.* 14:1–63.

Kennakin, T., and C. Boselli. 1989. Pharmacological discrimination between receptor heterogeneity and allosteric interaction: resultant analysis of gallamine and pirenzepine antagonism of muscarinic response in rat trachea. *J. Pharmacol. Exp. Ther.* 250:944–952.

Kozell, L. B., C. A. Machida, R. L. Neve, and K. A. Neve. 1994. Chimeric D1/D2 dopamine receptors. Distinct determinants of selective efficacy, potency, and signal transduction. *J. Biol. Chem.* 269:30299–30306.

Kriwacki, R. W., L. Hengst, L. Tennant, S. I. Reed, and P. E. Wright. 1996. Structural studies of p21Waf1/Cip1/Sdi1 in the free and Cdk2-bound state: conformational disorder mediates binding diversity. *Proc. Natl. Acad. Sci. USA.* 93:11504–11509.

Krogh, A., B. Larsson, G. von Heijne, and E. L. Sonnhammer. 2001. Predicting transmembrane protein topology with a hidden Markov model. *J. Mol. Biol.* 305:567–580.

Kukhtina, V. V., C. Weise, T. A. Muranova, V. G. Starkov, P. Franke, F. Hucho, S. Wnendt, C. Gillen, V. I. Tsetlin, and Y. N. Utkin. 2000. Muscarinic toxin-like proteins from cobra venom. *Eur. J. Biochem.* 267:6784–6789.

Kuo, R. C., G. T. Baxter, L. Alajoki, D. L. Miller, J. M. Libby, and J. C. Owicki. 1993. A metabolic view of receptor activation in cultured cells following cryopreservation. *Cryobiology.* 30:386–395.

Kurtenbach, E., C. A. Curtis, E. K. Pedder, A. Aitken, A. C. Harris, and E. C. Hulme. 1990. Muscarinic acetylcholine receptors. Peptide sequencing identifies residues involved in antagonist binding and disulfide bond formation. *J. Biol. Chem.* 265:13702–13708.

Kyte, J., and R. F. Doolittle. 1982. A simple method for displaying the hydropathic character of a protein. *J. Mol. Biol.* 157:105–132.

Lanzafame, A., A. Christopoulos, and F. Mitchelson. 1997. Three allosteric modulators act at a common site, distinct from that of competitive antagonists, at muscarinic acetylcholine M2 receptors. *J. Pharmacol. Exp. Ther.* 282:278–285.

Lau, S. H., J. Rivier, W. Vale, E. T. Kaiser, and F. J. Kezdy. 1983. Surface properties of an amphiphilic peptide hormone and of its analog: corticotropin-releasing factor and sauvagine. *Proc. Natl. Acad. Sci. USA.* 80:7070–7074.

Lauffenburger, D. A., and J. J. Linderman. 1993. Receptors: Models for Binding, Trafficking and Signaling. Oxford University Press, New York.

Lazareno, S., and N. Birdsall. 1996. Quantitation of allosteric interactions. *Trends Pharmacol. Sci.* 17:443–444.

Lazaridis, T., and M. Karplus. 1997. ''New view'' of protein folding reconciled with the old through multiple unfolding simulations. *Science.* 278:1928–1931.

Lazovic, J. 1996. Selection of amino acid parameters for Fourier transform-based analysis of proteins. *Comput. Appl. Biosci.* 12:553–562.

Leckband, D. E., J. N. Israelachvili, F. J. Schmitt, and W. Knoll. 1992. Long-range attraction and molecular rearrangements in receptor-ligand interactions. *Science.* 255:1419–1421.

Leckband, D. E., F. J. Schmitt, J. N. Israelachvili, and W. Knoll. 1994. Direct force measurements of specific and nonspecific protein interactions. *Biochemistry.* 33:4611–4624.

Lee, N. H., and E. E. el-Fakahany. 1991. Allosteric antagonists of the muscarinic acetylcholine receptor. *Biochem. Pharmacol.* 42:199–205.

Levey, A. I. 1996. Muscarinic acetylcholine receptor expression in memory circuits: implications for treatment of Alzheimer disease. *Proc. Natl. Acad. Sci. USA.* 93:13541–13546.

Liao, C. F., A. P. Themmen, R. Joho, C. Barberis, M. Birnbaumer, and L. Birnbaumer. 1989. Molecular cloning and expression of a fifth muscarinic acetylcholine receptor. *J. Biol. Chem.* 264:7328–7337.

Limbird, L. E. 1986. Cell Surface Receptors: A Short Course on Theory and Methods. Martinius Nijhoff Publishers, Boston.

Lin, Q., H. S. Park, Y. Hamuro, C. S. Lee, and A. D. Hamilton. 1998. Protein surface recognition by synthetic agents: design and structural requirements of a family of artificial receptors that bind to cytochrome c. *Biopolymers*. 47:285–297.

Lio, P., and M. Vannucci. 2000. Wavelet change-point prediction of transmembrane proteins. *Bioinformatics*. 16:376–382.

Lumry, R. 1995. On the interpretation of data from isothermal processes. *Methods Enzymol*. 259:628–720.

Ma, J., and M. Karplus. 1997. Molecular switch in signal transduction: reaction paths of the conformational changes in ras p21. *Proc. Natl. Acad. Sci. USA*. 94:11905–11910.

Madan, R. N. 1993. All poles, maximum entropy spectra. *In* Maximum Entropy and Bayesian Methods. A. Mohananad-Djafaro and G. Demoments, editors. Kluwar, Dardrecht, The Netherlands. 49–54.

Makhatadze, G. I., and P. L. Privalov. 1993. Contribution of hydration to protein folding thermodynamics. I. The enthalpy of hydration. *J. Mol. Biol*. 232:639–659.

Makino, S., and I. D. Kuntz. 1997. Automated flexible ligand docking method and its application for data base search. *J. Comput. Chem*. 18:1812–1825.

Mallat, S. 1989. Multiresolution approximation and wavelets. *Trans. Amer. Math. Soc*. 315:69–88.

Manavalen, P., and P. K. Ponnuswamy. 1978. Hydrophobic character of amino acid residues in globular proteins. *Nature*. 275:673–674.

Mandell, A. J. 1983. From chemical homology to topological temperature: a notion relating the structure and function of polypeptides. *In* Synergetics of the Brain. E. Basar, H. Flohr, H. Haken, and A. J. Mandell, editors. Springer-Verlag, Berlin. 365–376.

Mandell, A. J. 1984. Non-equilibrium behavior of some brain enzymes and receptor systems. *Annu. Rev. Pharmacol. Toxicol*. 24:237–274.

Mandell, A. J. 1986. Prime times: the distribution of singularities in hydrophobic free energy of proteins. *In* Perspectives in Nonlinear Dynamics. M. F. Shlesinger, R. Cawley, A. W. Saenz, and W. Zachary, editors. World Scientific, Singapore. 259–278.

Mandell, A. J. 1987. The source and characteristics of normal modes in molecular biology. *In* Synergetics, Order and Chaos. M. G. Velarde, editor. World Scientific, Singapore. 351–367.

Mandell, A. J., M. J. Owens, K. A. Selz, W. N. Morgan, M. F. Shlesinger, and C. B. Nemeroff. 1998a. Mode matches in hydrophobic free energy eigenfunctions predict peptide-protein interactions. *Biopolymers*. 46:89–101.

Mandell, A. J., and P. V. Russo. 1981. Striatal tyrosine hydroxylase activity: multiple conformational kinetic oscillators and product concentration frequencies. *J. Neurosci*. 1:380–389.

Mandell, A. J., P. V. Russo, and B. W. Blomgren. 1987. Geometric universality in brain allosteric protein dynamics; complex hydrophobic transformation predicts mutual recognition by polypeptides and proteins. *Ann. N. Y. Acad. Sci*. 504:88–117.

Mandell, A. J., and K. A. Selz. 1997. Entropy conservation as h(T(μ)) approximately lambda(μ) (+)d(μ) in neurobiological dynamical systems. *Chaos*. 7:67–81.

Mandell, A. J., K. A. Selz, M. J. Owens, M. F. Shlesinger, B. Kinkead, D. A. Gutman, and B. S. Arguragi. 2003. Cellular and behavioral effects of D2 dopamine receptor hydrophobic eigenmode-targeted peptide ligands. *Neuropsychopharmacology*. 26:S98–S107.

Mandell, A. J., K. A. Selz, M. J. Owens, M. F. Shlesinger, D. A. Gutman, and V. Arcuragi. 2001. Hydrophobic mode-targeted, algorithmically designed peptide ligands as modulators of protein thermodynamic structure and function. *In* Drug-Receptor Thermodynamics: Introduction and Applications. R. Raffa, editor. Wiley & Sons, New York. 655–700.

Mandell, A. J., K. A. Selz, and M. Shlesinger. 1997a. Wavelet transformation of protein hydrophobicity sequences suggests their memberships in structural families. *Physica A*. 244:254–262.

Mandell, A. J., K. A. Selz, and M. F. Shlesinger. 1997b. Hydrophobic free energy eigenfunctions help define continuous wavelet transformations of amino acid sequences of protein families. *Proc. Int. Sch. Physics ''Enrico Fermi''*. 134:175–191.

Mandell, A. J., K. A. Selz, and M. F. Shlesinger. 1997c. Mode matches and their locations in the hydrophobic free energy sequences of peptide ligands and their receptor eigenfunctions. *Proc. Natl. Acad. Sci. USA*. 94:13576–13581.

Mandell, A. J., K. A. Selz, and M. F. Shlesinger. 1998b. Transformational homologies in amino acid sequences suggest membership in protein families. *J. Stat. Phys*. 93:673–697.

Mandell, A. J., K. A. Selz, and M. F. Shlesinger. 2000a. Predicting peptide-receptor, peptide-protein and chaperone-protein binding using patterns in amino acid hydrophobic free energy sequences. *J. Phys. Chem. B*. 104:3953–3959.

Mandell, A. J., K. A. Selz, and M. F. Shlesinger. 2000b. Protein binding predictions from amino acid primary sequence hydrophobicity. *J. Mol. Liq*. 86:163–171.

Matsui, H., S. Lazareno, and N. J. Birdsall. 1995. Probing of the location of the allosteric site on m1 muscarinic receptors by site-directed mutagenesis. *Mol. Pharmacol*. 47:88–98.

May, R. M. 1974. Biological populations with nonoverlapping generations: stable points, stable cycles, and chaos. *Science*. 186:645–647.

McConnell, H. M., J. C. Owicki, J. W. Parce, D. L. Miller, G. T. Baxter, H. G. Wada, and W. Pitchford. 1992. The cytosensor microphysiometer: biological applications of silicon technology. *Science*. 257:1906–1912.

McKinney, M., and J. T. Coyle. 1991. The potential for muscarinic receptor subtype-specific pharmacotherapy for Alzheimer's disease. *Mayo Clin. Proc*. 66:1225–1237.

Mijares, A., D. Lebesgue, J. Argibay, and J. Hoebeke. 1996. Anti-peptide antibodies sensitive to the ''active'' state of the B2-adrenergic receptor. *FEBS Lett*. 399:188–191.

Mijares, A., D. Lebesgue, G. Wallukat, and J. Hoebeke. 2000. From agonist to antagonist: fab fragments of an agonist-like monoclonal anti-beta$_2$-adrenoceptor antibody behave like antagonists. *Mol. Pharmacol*. 58:373–379.

Milner-White, E. J., and R. Poet. 1987. Loops, bulges, turns and hairpins in proteins. *Trends Biochem. Sci*. 12:189–192.

Monne, M., M. Hermansson, and G. von Heijne. 1999. A turn propensity scale for transmembrane helices. *J. Mol. Biol*. 288:141–145.

Mrzljak, L., A. I. Levey, S. Belcher, and P. S. Goldman-Rakic. 1998. Localization of the m2 muscarinic acetylcholine receptor protein and mRNA in cortical neurons of the normal and cholinergically deafferented rhesus monkey. *J. Comp. Neurol*. 390:112–132.

Murray, K. B., D. Gorse, and J. M. Thornton. 2002. Wavelet transforms for the characterization and detection of repeating motifs. *J. Mol. Biol*. 316:341–363.

Naylor, L., R. Woodward, S. Daniell, C. Coley, and P. Strange. 1995. Determinants of ligand binding at the D2 dopamine receptor. *Biochem. Soc. Trans*. 23:87–91.

Neve, K. A., and B. L. Wiens. 1995. Four ways of being an agonist: multiple sequence determinants of efficacy at D2 dopamine receptors. *Biochem. Soc. Trans*. 23:112–116.

Nilsson, I., and G. von Heijne. 1998. Breaking the camel's back: proline-induced turns in a model transmembrane helix. *J. Mol. Biol*. 284:1185–1189.

Nirenberg, M. J., J. Chan, R. A. Vaughan, G. R. Uhl, M. J. Kuhar, and V. M. Pickel. 1997. Immunogold localization of the dopamine transporter: an ultrastructural study of the rat ventral tegmental area. *J. Neurosci*. 17:5255–5262.

Norris, J. D., L. A. Paige, D. J. Christensen, C. Y. Chang, M. R. Huacani, D. Fan, P. T. Hamilton, D. M. Fowlkes, and D. P. McDonnell. 1999. Peptide antagonists of the human estrogen receptor. *Science*. 285:744–746.

Nozaki, Y., and C. Tanford. 1971. The solubility of amino acids and two glycine peptides in aqueous ethanol and dioxane solutions. *J. Biol. Chem.* 246:2211–2217.

Numa, S., K. Fukuda, T. Kubo, A. Maeda, I. Akiba, H. Bujo, J. Nakai, M. Mishina, and H. Higashida. 1988. Molecular basis of the functional heterogeneity of the muscarinic acetylcholine receptor. *Cold Spring Harb. Symp. Quant. Biol.* 53:295–301.

Olianas, M. C., A. Ingianni, C. Maullu, A. Adem, E. Karlsson, and P. Onali. 1999. Selectivity profile of muscarinic toxin 3 in functional assays of cloned and native receptors. *J. Pharmacol. Exp. Ther.* 288:164–170.

Olianas, M. C., C. Maullu, A. Adem, E. Mulugeta, E. Karlsson, and P. Onali. 2000. Inhibition of acetylcholine muscarinic M(1) receptor function by the M(1)-selective ligand muscarinic toxin 7 (MT-7). *Br. J. Pharmacol.* 131:447–452.

Ott, E., T. Sauer, and J. A. Yorke. 1994. Coping with Chaos. Wiley, New York.

Owens, M. J., W. N. Morgan, S. J. Plott, and C. B. Nemeroff. 1997. Neurotransmitter receptor and transporter binding profile of antidepressants and their metabolites. *J. Pharmacol. Exp. Ther.* 283:1305–1322.

Palczewski, K., T. Kumasaka, T. Hori, C. A. Behnke, H. Motoshima, B. A. Fox, I. Le Trong, D. C. Teller, T. Okada, and R. E. Stenkamp. 2000. Crystal structure of rhodopsin: a G-protein coupled receptor. *Science.* 289:739–745.

Park, S., M. E. Johnson, and L. W. Fung. 2000. NMR analysis of secondary structure and dynamics of a recombinant peptide from the N-terminal region of human erythroid alpha-spectrin. *FEBS Lett.* 485:81–86.

Pashley, R. M., P. M. McGuiggan, B. W. Ninham, and D. F. Evans. 1985. Attractive forces between uncharged hydrophobic surfaces: direct measurement in aqueous solution. *Science.* 229:1088–1089.

Penel, S., R. G. Morrison, R. J. Mortishire-Smith, and A. J. Doig. 1999. Periodicity in alpha-helix lengths and C-capping preferences. *J. Mol. Biol.* 293:1211–1219.

Peralta, E. G., J. W. Winslow, G. L. Peterson, D. H. Smith, A. Ashkenazi, J. Ramachandran, M. I. Schimerlik, and D. J. Capon. 1987. Primary structure and biochemical properties of an M2 muscarinic receptor. *Science.* 236:600–605.

Perry, T. L., S. Hansen, and J. Kennedy. 1975. CSF amino acids and plasma-CSF amino acid ratios in adults. *J. Neurochem.* 24:587–589.

Press, W. H. B.P. Flannery, S. A. Teukolsky, and W. T. Vetterling. 1988. Numerical Recipes in C; The Art of Scientific Computing. Cambridge University Press, Cambridge.

Priestly, M. D. 1981. Spectral Analysis and Time Series. Academic Press, San Diego.

Privalov, P. L. 1987. Protein stability and hydrophobic interactions. *Biofizika.* 32:742–760.

Privalov, P. L. 1989. Thermodynamic problems of protein structure. *Annu. Rev. Biophys. Biophys. Chem.* 18:47–69.

Privalov, P. L., and S. J. Gill. 1988. Stability of protein structure and hydrophobic interaction. *Adv. Protein Chem.* 39:191–234.

Proska, J., and S. Tucek. 1995. Competition between positive and negative allosteric effectors on muscarinic receptors. *Mol. Pharmacol.* 48:696–702.

Ptitsyn, O. B., V. E. Bychkova, and V. N. Uversky. 1995. Kinetic and equilibrium folding intermediates. *Philos. Trans. R. Soc. Lond. B Biol. Sci.* 348:35–41.

Qu, Y., J. C. Rogers, S. F. Chen, K. A. McCormick, T. Scheuer, and W. A. Catterall. 1999. Functional roles of the extracellular segments of the sodium channel alpha subunit in voltage-dependent gating and modulation by beta1 subunits. *J. Biol. Chem.* 274:32647–32654.

Rackovsky, S. 1998. ''Hidden'' sequence periodicities and protein architecture. *Proc. Natl. Acad. Sci. USA.* 95:8580–8584.

Radzicka, A., and R. Wolfenden. 1988. Comparing the polarities of the amino acids: side-chain distribution coefficients between the vapor phase, cyclohexane, l-octanol and neutral aqueous solution. *Biochemistry.* 27:1664–1670.

Richards, F. M., and T. Richmond. 1977. Solvents, interfaces and protein structure. *Ciba Found. Symp.* 60:23–45.

Romero, P., Z. Obradovic, C. R. Kissinger, J. E. Villafranca, E. Garner, S. Guilliot, and A. K. Dunker. 1998. Thousands of proteins likely to have long disordered regions. *Pac. Symp. Biocomput.* 437–448.

Romero, P., Z. Obradovic, X. Li, E. C. Garner, C. J. Brown, and A. K. Dunker. 2001. Sequence complexity of disordered protein. *Proteins.* 42:38–48.

Rondard, P., and H. Bedouelle. 2000. Mutational scanning of a hairpin loop in the tryptophan synthase beta-subunit implicated in allostery and substrate channeling. *Biol. Chem.* 381:1185–1193.

Rose, G. D. 1978. Prediction of chain turns in globular proteins on a hydrophobic basis. *Nature.* 272:586–590.

Rose, G. D., and S. Roy. 1980. Hydrophobic basis of packing in globular proteins. *Proc. Natl. Acad. Sci. USA.* 77:4643–4647.

Rose, G. D., and D. B. Wetlaufer. 1977. The number of turns in globular proteins. *Nature.* 268:769–770.

Russo, P. V., and A. J. Mandell. 1984. Metrics from nonlinear dynamics adapted for characterizing the behavior of nonequilibrium enzymatic rate functions. *Anal. Biochem.* 139:91–99.

Sandak, B., R. Nussinov, and H. J. Wolfson. 1998. A method for biomolecular structural recognition and docking allowing conformational flexibility. *J. Comput. Biol.* 5:631–654.

Sanger, F. 1952. Amino acid sequences are unique in polypeptides and proteins. *Adv. Prot. Chem.* 7:1–67.

Schiffer, M., and A. B. Edmundson. 1967. Use of helical wheels to represent the structures of proteins and to identify segments with helical potential. *Biophys. J.* 7:121–135.

Schwartz, T. W., and M. M. Rosenkilde. 1996. Is there a ''lock'' for all agonist ''keys'' in 7TM receptors? *Trends Pharmacol. Sci.* 17:213–216.

Selz, K. A., and A. J. Mandell. 1991. Bernoulli partition-equivalence of intermittent neuronal discharge patterns. *Int J. Bifurcat. Chaos.* 1:717–722.

Selz, K. A., A. J. Mandell, C. M. Anderson, W. P. Smotherman, and M. Teicher. 1995. Distribution of local Mandelbrot-Hurst exponents: motor activity in cocaine treated fetal rats and manic depressive patients. *Fractals.* 3:893–904.

Selz, K. A., A. J. Mandell, and M. F. Shlesinger. 1998. Hydrophobic free energy eigenfunctions of pore, channel, and transporter proteins contain beta-burst patterns. *Biophys. J.* 75:2332–2342.

Sharp, K. A., A. Nicholls, R. F. Fine, and B. Honig. 1991a. Reconciling the magnitude of the microscopic and macroscopic hydrophobic effects. *Science.* 252:106–109.

Sharp, K. A., A. Nicholls, R. Friedman, and B. Honig. 1991b. Extracting hydrophobic free energies from experimental data: relationship to protein folding and theoretical models. *Biochemistry.* 30:9686–9697.

Shoemaker, B. A., J. Wang, and P. G. Wolynes. 1997. Structural correlations in protein folding funnels. *Proc. Natl. Acad. Sci. USA.* 94:777–782.

Shu, W., J. Liu, H. Ji, L. Radigen, S. Jiang, and M. Lu. 2000. Helical interactions in the HIV-1 gp41 core reveal structural basis for the inhibitory activity of gp41 peptides. *Biochemistry.* 39:1634–1642.

Simpson, M. M., J. A. Ballesteros, V. Chiappa, J. Chen, M. Suehiro, D. S. Hartman, T. Godel, L. A. Snyder, T. P. Sakmar, and J. A. Javitch. 1999. Dopamine D4/D2 receptor selectivity is determined by A divergent aromatic microdomain contained within the second, third, and seventh membrane-spanning segments. *Mol. Pharmacol.* 56:1116–1126.

Spencer, R. W. 1998. High-throughput screening of historic collections: observations on file size, biological targets, and file diversity. *Biotechnol. Bioeng.* 61:61–67.

Stahl, M., and H. J. Bohm. 1998. Development of filter functions for protein-ligand docking. *J. Mol. Graph. Model.* 16:121–132.

Stillinger, F. H. 1977. Theoretical approaches to the intermolecular nature of water. *Philos. Trans. R. Soc. Lond. B Biol. Sci.* 278:97–112.

Strang, G. 1993. Wavelet transformation versus Fourier transformation. *Bull. Am. Math Soc.* 28:288–305.

Takeuchi, Y., E. F. Shands, D. D. Beusen, and G. R. Marshall. 1998. Derivation of a three-dimensional pharmacophore model of substance P antagonists bound to the neurokinin-1 receptor. *J. Med. Chem.* 41:3609–3623.

Tanford, C. 1980. The Hydrophobic Effect. Wiley, New York.

Tsao, Y. H., D. F. Evans, and H. Wennerstrom. 1993. Long-range attractive force between hydrophobic surfaces observed by atomic force microscopy. *Science.* 262:547–550.

Tucek, S., and J. Proska. 1995. Allosteric modulation of muscarinic acetylcholine receptors. *Trends Pharmacol. Sci.* 16:205–212.

Ulloa-Aguirre, A., and P. M. Conn. 2000. G protein-coupled receptors and G proteins. *In* Principles of Molecular Recognition. P. M. Conn and A. R. Means, editors. Humana, Totowa, NJ. 3–25.

Unwin, N. 1993. Nicotinic acetylcholine receptor at 9 Å resolution. *J. Mol. Biol.* 229:1101–1124.

Vaughan, R. A., J. D. Gaffaney, J. R. Lever, M. E. Reith, and A. K. Dutta. 2001. Dual incorporation of photoaffinity ligands on dopamine transporters implicates proximity of labeled domains. *Mol. Pharmacol.* 59:1157–1164.

von Heijne, G. 1991. Proline kinks in transmembrane alpha-helices. *J. Mol. Biol.* 218:499–503.

Wang, H. L., K. Ohno, M. Milone, J. M. Brengman, A. Evoli, A. P. Batocchi, L. T. Middleton, K. Christodoulou, A. G. Engel, and S. M. Sine. 2000. Fundamental gating mechanism of nicotinic receptor channel revealed by mutation causing a congenital myasthenic syndrome. *J. Gen. Physiol.* 116:449–462.

Watanabe, M., J. Rosenbusch, T. Schirmer, and M. Karplus. 1997. Computer simulations of the OmpF porin from the outer membrane of *Escherichia coli*. *Biophys. J.* 72:2094–2102.

Wess, J., T. I. Bonner, F. Dorje, and M. R. Brann. 1990. Delineation of muscarinic receptor domains conferring selectivity of coupling to guanine nucleotide-binding proteins and second messengers. *Mol. Pharmacol.* 38:517–523.

Wickerhauser, M. V. 1994. Adapted Wavelet Analysis from Theory to Software. A. K. Peters, Wellesley, MA.

Wold, S. 1965. Bibliography on Time-Series and Stochastic Processes. Oliver and Boyd, Edinburgh.

Wood, M. D., K. L. Murkitt, M. Ho, J. M. Watson, F. Brown, A. J. Hunter, and D. N. Middlemiss. 1999. Functional comparison of muscarinic partial agonists at muscarinic receptor subtypes hM1, hM2, hM3, hM4 and hM5 using microphysiometry. *Br. J. Pharmacol.* 126:1620–1624.

Woodward, R., S. J. Daniell, P. G. Strange, and L. H. Naylor. 1994. Structural studies on D2 dopamine receptors: mutation of a histidine residue specifically affects the binding of a subgroup of substituted benzamide drugs. *J. Neurochem.* 62:1664–1669.

Wouters, J., G. Baudoux, E. Depiereux, and P. Fischer. 2000. Analysis of transmembrane helices in protein sequences using wavelet-based hydropathic plots. fischer@math.u-bordeaux,fr.

Wright, P. E., and H. J. Dyson. 1999. Intrinsically unstructured proteins: reassessing the protein structure-function paradigm. *J. Mol. Biol.* 293:321–331.

Yaglom, A. M. 1962. An Introduction to the Theory of Stationary Random Functions. Prentice-Hall, Englewood Cliffs, NJ.

Yang, A. S., and B. Honig. 1995. Free energy determinants of secondary structure formation: I. Alpha-helices. *J. Mol. Biol.* 252:351–365.

Zamyatnin, A. A. 1984. Amino acid, peptide and protein volume in solution. *Annu. Rev. Biophys. Bioeng.* 13:145–165.

Zysk, J. R., and W. R. Baumbach. 1998. Homogeneous pharmacologic and cell-based screens provide diverse strategies in drug discovery: somatostatin antagonists as a case study. *Comb. Chem. High Throughput Screen.* 1:171–183.